

**DEVELOPMENT OF BRAGG FIBER SENSOR FOR
CORROSION DETECTION**

TAN CAI HUI

**FACULTY OF ENGINEERING
UNIVERSITY OF MALAYA
KUALA LUMPUR**

2020

**DEVELOPMENT OF BRAGG FIBER SENSOR FOR
CORROSION DETECTION**

TAN CAI HUI

**THESIS SUBMITTED IN FULFILMENT OF THE
REQUIREMENTS FOR THE DEGREE OF DOCTOR OF
PHILOSOPHY**

**FACULTY OF ENGINEERING
UNIVERSITY OF MALAYA
KUALA LUMPUR**

2020

UNIVERSITY OF MALAYA
ORIGINAL LITERARY WORK DECLARATION

Name of Candidate: TAN CAI HUI

Matric No: KHA 130014

Name of Degree: Doctor of Philosophy

Title of ~~Project~~ ~~Paper~~ ~~Research~~ ~~Report~~ ~~Dissertation~~ ~~Thesis~~ (“this Work”):
Development of Bragg Fiber Sensor for Corrosion Detection

Field of Study: Electrical Engineering

I do solemnly and sincerely declare that:

- (1) I am the sole author/writer of this Work;
- (2) This Work is original;
- (3) Any use of any work in which copyright exists was done by way of fair dealing and for permitted purposes and any excerpt or extract from, or reference to or reproduction of any copyright work has been disclosed expressly and sufficiently and the title of the Work and its authorship have been acknowledged in this Work;
- (4) I do not have any actual knowledge nor do I ought reasonably to know that the making of this work constitutes an infringement of any copyright work;
- (5) I hereby assign all and every rights in the copyright to this Work to the University of Malaya (“UM”), who henceforth shall be owner of the copyright in this Work and that any reproduction or use in any form or by any means whatsoever is prohibited without the written consent of UM having been first had and obtained;
- (6) I am fully aware that if in the course of making this Work I have infringed any copyright whether intentionally or otherwise, I may be subject to legal action or any other action as may be determined by UM.

Candidate’s Signature

Date:

Subscribed and solemnly declared before,

Witness’s Signature

Date:

Name:

Designation:

DEVELOPMENT OF BRAGG FIBER SENSOR FOR CORROSION

DETECTION

ABSTRACT

Steel corrosion has posed one of the major structural defects in the civil society today. Conventional methods for corrosion monitoring involve high maintenance cost and destructive methods with low accuracy. Recently, Fiber Bragg gratings (FBG) sensor with its high sensitivity in measuring strain and temperature have been widely studied and used in structural health monitoring (SHM). A non-destructive corrosion detection approach based on FBG sensors was developed and tested to monitor corrosion in this research work. The principle of FBG sensing is based on Bragg wavelength shifts that from the corrosion process that induced strain on the FBG due to mechanical expansion. The first method that had been carried out in this study was the Polydimethylsiloxane (PDMS) coated FBG; while second method was the development of new coating material with better sensitivity for corrosion detection, which was a mixture of PDMS strain sensitive materials and pH sensitive hydrogel. FBG were etched in hydrofluoric acid (HF) near to the core of 9.7 μm to enhance the FBG sensitivity before the application of a coating material. FBG sensors were embedded on the rebar specimen. This is to monitor the strain expansion caused by corrosion process. Their performances were then being monitored by observing the Bragg wavelength shift via FBGA. Generally, PDMS-hydrogel sensor better sensitivity for corrosion monitoring at 1.97 nm / mm / year followed by FBG-PDMS at 1.65 nm / mm / year, as compared to non-coated FBG at 1.21 nm / mm / year. Overall, this research work have revealed and proven that it is feasible to develop FBG sensors as a real-time non-destructive structural health monitoring system in civil engineering.

Keywords: FBG, Corrosion, SHM , PDMS, Hydrogel.

University of Malaya

DEVELOPMENT OF BRAGG FIBER SENSOR FOR CORROSION

DETECTION

ABSTRAK

Pengaratian besi dikenali sebagai kecacatan struktur yang besar di dalam bidang kejuruteraan sivil. Kaedah konvensional untuk mengawasi proses pengaratian melibatkan kos penyelenggaraan yang tinggi dan kaedah musnah yang tidak tepat. Sensor Fiber Bragg gratings (FBG) yang sangat peka dalam mengukur strain dan haba telah digunakan secara meluas dalam mengawasi struktur kesihatan (SHM). Di dalam kerja penyelidikan thesis ini, kaedah pengesanan pengaratian tidak musnah menggunakan sensor FBG telah dibangunkan dan diuji untuk mengawasi proses pengaratian. Prinsip pengesanan adalah berdasarkan anjakan panjang gelombang Bragg yang dihasilkan daripada proses pengaratian yang mencetuskan strain di dalam FBG disebabkan pengembangan mekanikal. Kaedah pertama yang telah di uji di dalam penyelidikan ini adalah menggunakan FBG bersalut Polydimethylsiloxane (PDMS), sementara kaedah kedua adalah pembangunan bahan penyalut yang baru yang lebih peka untuk mengenal pasti proses pengaratian, iaitu campuran hidrogel yang peka kepada pH bersama-sama dengan PDMS yang peka kepada perubahan strain. FBG telah dipunat di dalam asid hidroflorik sehingga lapisan teras berukuran $9.7 \mu\text{m}$ untuk meningkatkan kepekaan FBG sebelum disalut dengan bahan penyalut. Sensor FBG kemudian telah dimasukkan ke dalam spesimen rebar untuk mengawasi pengembangan strain yang di sebabkan oleh process pengaratian. Prestasi sensor kemudian diperhatikan berdasarkan anjakan panjang gelombang Bragg menggunakan FBGA. Secara amnya, sensor PDMS-hidrogel mempunyai prestasi yang lebih peka untuk mengawasi proses pengaratian dengan anjakan gelombang Bragg sebanyak $1.97 \text{ nm / mm / tahun}$ di ikuti oleh FBG-PDMS dengan $1.65 \text{ nm / mm / tahun}$ di dibandingkan dengan FBG yang tidak bersalut yang menunjukkan anjakan gelombang Bragg sebanyak $1.21 \text{ nm / mm / tahun}$. Secara

keseluruhan, penyelidikan ini membuktikan bahawa pembangunan sensor FBG boleh dilaksanakan sebagai sistem pengawasan masa nyata tidak musnah SHM di dalam kejuruteraan sivil.

Kata kunci: FBG, Pengaratan, SHM , PDMS, Hidrogel

University of Malaya

ACKNOWLEDGEMENTS

I would like to express my utmost gratitude and thanks to my supervising lecturer, Professor Dr. Faisal Rafiq Mahmad Adikan and Professor Dr. Shee Yu Gang and Associate Professor Dr. Yap Boon Kar as for their research funding support, endurance, encouragement, and patient guidance during the course of this project. Their advices have guided and helper me through various obstacles and difficulties.

I would also like to express my heartfelt appreciation to my research group, the ILRG research group lab mate who has both directly or indirectly offered the necessity help and suggestions and support, contributing towards the successful completion of this project. We are always working closely and motivating each other.

Special thanks to my beloved friends and family for giving me the encouragement, understanding, support and care. Thank you for the boundless love!

TABLE OF CONTENTS

Abstract	iii
Abstrak	v
Acknowledgements	vii
Table of Contents	viii
List of Figures	xi
List of Tables.....	xiii
List of Symbols and Abbreviations.....	xiv
CHAPTER 1: INTRODUCTION	16
1.1 Background	16
1.1.1 Structural Health Monitoring	16
1.1.2 Conventional Method for Corrosion Monitoring	18
1.2 Problem Statement	19
1.3 Objective	20
1.4 Scope Of Work	20
1.5 Thesis Outline	21
CHAPTER 2: LITERATURE REVIEW	22
2.1 Introduction.....	22
2.2 Corrosion.....	23
2.3 Effects Of Corrosion	23
2.4 Process Of Corrosion	24
2.5 Types Of Corrosion.....	25
2.5.1 General / Uniform Corrosion	25
2.5.2 Stress Corrosion Cracking (SCC).....	26
2.5.3 Corrosion Stress	28
2.6 Methods Of Corrosion Detection.....	29

2.7 Optical Fiber	31
2.8 Optical Fiber Sensors	31
2.8.1 Discrete Fiber Sensor	33
2.8.2 Distributed Fiber Sensor	34
2.9 Fiber Bragg Grating (FBG) Sensor	35
2.10 Principle of Operation	36
2.11 Theory and Models of FBG	37
2.12 Advantages of FBG Sensors Over Conventional Sensors	40
2.13 Polydimethylsiloxane (PDMS)	41
2.14 PH Sensitive Hydrogel	43
CHAPTER 3: RESEARCH METHODOLOGY	47
3.1 Introduction	47
3.2 Research Methodology Flow Chart	47
3.3 FBG Etching	49
3.4 FBG with PDMS Coating	52
3.5 Mixture of PDMS and Hydrogel Coating	56
3.6 Corrosion Weight Loss Test	58
3.7 Summary	59
CHAPTER 4: RESULTS AND DISCUSSION	60
4.2 FBG Etching	60
4.2.1 Sensitivity Characterization of Etched Fibers	68
4.3 Study of Evanescent Field in Etched Fiber	70
4.4 PDMS Coating Characterization	73
4.4.1 Corrosion Rate	74
4.4.2 Results and Discussion	75
4.5 Hydrogel-Coated FBG Characterization	81

4.5.1 Results and Discussion	83
4.6 Chapter Summary	86
CHAPTER 5: CONCLUSION AND FUTURE RECOMMENDATION	87
5.1 Conclusion	87
5.2 Future Works	89
REFERENCES.....	90
List of Publications and Papers Presented	988

University of Malaya

LIST OF FIGURES

Figure 2.1: Uniform Corrosion (Al-Sulaimani, Kaleemullah, Basunbul, & Rasheeduzzafar, 1990).	26
Figure 2.2: Stress Corrosion Cracking (Nishimura & Maeda, 2004).	27
Figure 2.3: Condition for Stress Corrosion Cracking (Shoji et al., 2011).	28
Figure 2.4: Components of an Optical Fiber Sensor System (Muhammad Younus, Pankaj Chakrabarty & Mosharrafa Ahmad, 2015).	32
Figure 2.5: An optical fiber Bragg grating structure illuminated by broadband light (Pereira, 2016).	36
Figure 2.6: Electromagnetic wave interference (Majumder et al., 2008).	38
Figure 2.7: Bragg reflection wave shape (Majumder et al., 2008).	39
Figure 2.8: Chemical composition of PDMS (Zhongde Dai, Luca Ansaloni & Liyuan Deng, 2016).	42
Figure 2.9: Structure of hydrogel (Mahdavinia et al., 2004).	45
Figure 2.10: Swelling phenomena of a hydrogel (Mahdavinia et al., 2004).	45
Figure 3.1: Research methodology.	48
Figure 3.2: Experiment methodology flowchart 1.	49
Figure 3.3: FBG etching experiment setup.	50
Figure 3.4: FBG before and after etched.	52
Figure 3.5: PDMS solution preparation.	53
Figure 3.6: PDMS solution on aluminium plate.	54
Figure 3.7: Rebar mounted on an aluminum plate.	54
Figure 3.8: A thin PDMS layer coated FBG fiber.	55
Figure 3.9: Flowchart 2 experimental.	55
Figure 3.10: PDMS-hydrogel solution preparation.	57

Figure 3.11: Experiment setup.	58
Figure 4.1: FBG wavelength (1547.54 nm) at 18 minutes of etching.	61
Figure 4.2: FBG wavelength (1547.24 nm) at 19 minutes 10 seconds of etching.	61
Figure 4.3: FBG wavelength (1547.38 nm) at T0.	62
Figure 4.4: FBG diameter by etching time with error bars.	63
Figure 4.5: SEM measurements on, (a) un-etched FBG, (b) 90 μ m etched, (c) 56.9 μ m etched, (d) 28.2 μ m etched, (e) 12.5 μ m etched, (f) 11.2 μ m etched, (g) 10.9 μ m etched, (h) 10.7 μ m etched, (i) 9.7 μ m etched.	68
Figure 4.6: Bragg wavelength shift for different FBG thickness under different ethanol concentration.	69
Figure 4.7: COMSOL simulation on etched and un-etched fiber.	71
Figure 4.8: Power distribution for different FBG diameter.	72
Figure 4.9: Corroded Rebar.	73
Figure 4.10: Wavelength shift and corrosion rate by days.	75
Figure 4.11: Wavelength shift by corrosion rate.	76
Figure 4.12: PDMS mechanism.	78
Figure 4.13: Relationship between corrosion rate and strain induced by time.	80
Figure 4.14: Strain induced vs corrosion rate.	80
Figure 4.15: Structure of PDMS-Hydrogel coated in etched FBG.	82
Figure 4.16: FBG wavelength before and after coating at 1547.38 nm.	82
Figure 4.17: FBG wavelength shifts comparison PDMS and PDMS-Hydrogel sensor.	84
Figure 4.18: FBG wavelength shift by corrosion rate for PDMS and PDMS-Hydrogel sensor.	85

LIST OF TABLES

Table 2.1: Advantages of FBG Sensors.	40
Table 4.1: Corrosiveness Category under BS EN 12500:2000 for four common materials.	74
Table 5.1: The comparison of fabricated FBG sensors in this thesis work with the literature.	88

University of Malaya

LIST OF SYMBOLS AND ABBREVIATIONS

SHM	:	Structural health monitoring
FBG	:	Fiber Bragg grating
PDMS	:	Polydimethylsiloxane
NACE	:	National Association of Corrosion Engineers
SCC	:	Stress Corrosion Cracking
CR	:	Corrosion rate
TDM	:	Time-division multiplexing
WDM	:	Wavelength division multiplexing
NDT	:	Non-destructive testing
HF	:	Hydrofluoric acid
HCl	:	Hydrochloric acid
DI	:	Deionized water
ASE	:	Amplified Spontaneous Emission
OSA	:	Optical Spectrum Analyzer
SEM	:	Scanning Electron Microscopy
RI	:	Refractive index
ASTM	:	American Society for Testing and Materials
FWHM	:	Full-Width-Half-Maximum
Fe(OH) ₂	:	Iron (II) hydroxide
Fe(OH) ₃	:	Iron (III) hydroxide
W	:	Intensity
Λ	:	Grating period
E	:	Evanescent field
Fe	:	Iron
H ⁺	:	Hydrogen ion

T	:	Time
A	:	Area
D	:	Distance
μm	:	Micrometer
nm	:	Nanometer
n_{eff}	:	Refractive effective index
λ_{B}	:	Bragg wavelength
P_{sw}	:	Swelling pressure
ΔT	:	Temperature variation
$\Delta \varepsilon$:	Variation of the strain

University of Malaya

CHAPTER 1: INTRODUCTION

1.1 Background

Today, rebar and steel architectures serve as the mainstream construction structural support in the civil engineering field. The used of these materials tend to decay overtime due to corrosion which will eventually lead to building or road structure damages and collapse (Popoola, Grema, Latinwo, Gutti, & Balogun, 2013). The corrosion of rebar in the concrete structure is one of the main sources to a weakened structure.

Corrosion is undoubtedly a natural phenomenon and the National Associate of Corrosion Engineers (NACE) has defined corrosion as the deterioration of a material, usually a metal, resulted from a naturally occurring reaction with its surrounding environment.

The conventional method of corrosion inspection is rather time consuming. It is often costly and usually will cause additional damages. This is because corrosion can happen at any location that cannot be inspected visually. The method of the existing corrosion monitoring are costly as it uses a separate expensive infrastructure and it involves a large amount of commitment of time and labour. Despite it being costly, the method does not guarantee the full and accurate structural corrosion information that is being monitored (Majumder, Gangopadhyay, Chakraborty, Dasgupta, & Bhattacharya, 2008).

The monitoring of a structural health is rather essential because it feeds us the information of a road or building structural integrity. This information is useful in preventing severe structure deterioration and even lost of life (Tan, Shee, Yap, & Adikan, 2016). Structural Health Monitoring (SHM) is also commonly discussed and

researched for its advantages in its non-destructive monitoring mechanism. Furthermore, SHM serves in reducing maintenance costs and preventing an irreparable damage from occurring (Surre, Sun, & Grattan, 2013). Thus, the implementation of SHM systems are beneficial as it aids in repair and maintenance cost reduction.

1.1.1 Structural Health Monitoring

SHM is typically an engineering field concerned with the development of damage detection system to enhance the transition from scheduled maintenance to condition-based maintenance. It can also explained as the process that comprises of observing a civil structure over time using space and periodical measurements, feature extraction from these measurements and finally analyzing the results from those measurements to assess the current health state of the structural system (Hui, Charlebois, & Sun, 2018). The output of the whole process is periodical update of the capability of the structure to continue supporting the service it was intended to perform. The most fundamental importance of SHM includes detecting early safety risks, longer life spans and cost-efficiency (“4 Societal Benefits of Structural Health Monitoring (SHM),” n.d.).

Detecting Early Safety Risks: SHM has helped engineers to evaluate the potential future risks in civil engineering structures. This has mainly been applied to track the geological details of buildings, roads and other structures as well as structural corrosion. This enables professionals in the engineering field to detect early on incidences of ground movement, allowing them to mitigate risks arising from the defects or other disasters.

Longer Life Spans: the regular emergency and preventive maintenance carried out on civil infrastructures are aimed at increasing the longevity of the structures. New technologies and approaches that employ SHM enable engineers to maintain and build

longstanding structures like never before. The installed sensing technology provides more details on the structural health and prevents the accounts of human error.

Cost Efficiency: in addition to ensuring a longer life span and improving structural safety, SHM also reduces short-term and long-term costs associated with structural maintenance. Maintaining civil structures for more extended periods reduces the risks of structural damage as well as the overall maintenance costs.

1.1.2 Conventional Method for Corrosion Monitoring

Corrosion inspection is crucial structural monitoring for tower buildings and bridges. However, most of the conventional corrosion inspections are costly, time-consuming and with additional damages due to the destructive measurement method. The most common existing methods for analyzing corrosion are linear polarization resistance and weight loss coupons.

Linear polarization is a method to measure continuous corrosion rate. Specifically, polarization resistance method works by recording the current during anodic and cathodic reactions. During these reactions, polarization is referred to the change in the potential. This potential is then used to analyze the corrosion. However, there are some limitations by using this technique, as they require physical contact with the concrete structure. This method also depends on the area of the measurement which with only a small area it cannot represent the whole structural corrosion situation and this may lead to errors in corrosion analyzing (Devesh P. Kansara, Akshay P. Sorathiya & Himanshukumar R. Patel, 2018).

Weight loss is the simplest and presumably the oldest method for corrosion monitoring. It involves metal weight measurement followed by calculating the penetration rate of the weight loss based on the exposure time and exposed surface. It

requires a lot of manual interaction to collect the information. However, it is a destructive method to measure the rebar corrosion depth inside a structure (Devesh P. Kansara, Akshay P. Sorathiya & Himanshukumar R. Patel, 2018).

Another technique that can be utilized for assessment of corrosion in steel is the measurement of depth of carbonate or chloride profile in the concrete structure. Other well-known methods are chemical performance analysis of the samples that obtained from the concrete structures (Zeng et al., 2017). All these conventional methods are destructive as they require collection of samples from the structure for analysis to ascertain its health condition. These methods therefore call for scheduled maintenance which is costly and usually they do not provide accurate information on the extent of the damage (Smyrl, 1993).

Fiber Bragg gratings (FBG) with its great sensitivity to strain and temperature is receiving great attention lately as it is used to monitor the structural condition as real-time non-destructive sensors. It had been developed to sensors with various applications, such as strain/stress sensors, temperature sensors, vibration sensors, crack sensors, tilt-meter, displacement sensors and etc. It will be a great potential candidate in the development of corrosion sensors with proper coating and packaging.

1.2 Problem Statement

The most fundamental importance of SHM includes improved safety, early detection to avoid causalities due to structural failure, longer life spans and cost-efficiency. However, most of the conventional corrosion inspection is costly and time-consuming as well as it poses additional damages due to the destructive method (X. W. Ye, Su, & Han, 2014). Therefore, development of an effective non-destructive FBG system is crucial for a real-time corrosion monitoring system.

Development of corrosion sensors based on FBG will offer a non-destructive solution for corrosion monitoring. FBG need to be processed to fit the applications in corrosion sensing. Suitable coating materials need to be studied and characterized for FBG corrosion sensing. An optimized mixture of coating materials will be developed for the packaging of FBG corrosion sensor.

1.3 Objectives

The research work focuses on the development of FBG sensors for corrosion detection. The main intention in this work is to characterize sensitivity corrosion detection base on shifted wavelengths in FBG. The objectives of this research are as follows:

1. To develop non-destructive corrosion sensors based on FBG sensors.
2. To develop and characterize coating materials on FBG for corrosion sensing.
3. To compare the corrosion detection sensitivity of non-destructive sensor with conventional method.
4. To optimize the coating materials on FBG for corrosion sensing with high sensitivity.

1.4 Scope of Work

This research work focuses on the corrosion detection via FBG sensor for non-destructive SHM. FBG etching was carried out to improve its sensitivity, and coating materials are characterized and developed in this study for corrosion sensing. In addition, a new coating material which is sensitive to pH change has been developed to enhance the sensitivity in FBG sensor for corrosion detection. All the results are principally based on experimental work carried out in this research work.

1.5 Thesis Outline

This dissertation presents the development and characterization of FBG sensor coating for early corrosion detection. This research works are organized into 5 chapters. An introduction of the structural failure and importance of SHM in civil engineering, as well as the review on non-destructive sensor over conventional methods are given in chapter 1. In addition to that, the objectives of the research and scope of the work are also presented in this chapter.

In chapter 2, literature reviews on process and the impact of corrosion to the structural building, as well as the existing conventional method for corrosion inspection are discussed. The theoretical and operation principles of the FBG are also included in this chapter. This chapter end with the discussion on the coating material which was to enhance the sensitivity of FBG sensor for corrosion detection. The general preparation of FBG and the experimental techniques involved in this study as well as the general flow chart of the research work are presented in chapter 3.

Chapter 4 describes the results of this experiment works and are divided into few sub-sections. First section reported the effects of FBG etching as to enhance the sensitivity of FBG with ethanol concentration test supported data by COMSOL simulation. Temperature compensation for the FBG sensor was discussed in second section. Third section discussed the characterization and the sensitivity on PDMS FBG sensor to the corrosion detection; while fourth section focuses of a novel FBG sensor by a mixture of PDMS and hydrogel to further enhance the FBG sensor sensitivity for early corrosion detection. The results as in wavelength shifted and strain induced is also presented and analysed.

Chapter 5 concludes the overall research work done in this dissertation and envisages future work directions.

CHAPTER 2: LITERATURE REVIEW

2.1 Introduction

In civil engineering, most construction structures are supported by rebar or steel architectures, which lead to damages or collapses due to corrosion (Popoola et al., 2013). Rebar corrosion within concrete structures is one of the primary reasons which make an entire construction weakened. Corrosion is a naturally occurring phenomenon, commonly defined by the National Association of Corrosion Engineers (NACE) as the deterioration of a material, usually a metal that results from a reaction with the surrounding environment.

Corrosion inspection is time consuming, costly and often causes additional damages since corrosion can occur at any location that cannot be inspected visually. Existing conventional corrosion monitoring methods are always including high costs of having a separate infrastructure and large commitment of time or labour. Nevertheless, these methods cannot enable full and accurate information for the whole corrosion situation of the object being monitored (Majumder et al., 2008).

Therefore, SHM is very important and essential nowadays because it prevents severe deterioration by detection of abnormalities in the earliest possible stage (Tan et al., 2016). SHM is also commonly discussed and researched for its advantages in non-destructive monitoring. In addition, SHM contributes to reduced maintenance costs, and avoids irreparable damage from occurring (Surre et al., 2013). Thus, by implementing SHM systems, it helps to reduce the cost of repair and maintenance.

2.2 Corrosion

Corrosion can be defined as the destructive attack or deterioration of metallic materials and their alloys due to their interaction with the environment. Corrosion is an accumulative process that alters the surface property and fracture strength of structures, resulting in premature deterioration. This deterioration is as a result of electrochemical and chemical reactions that result from thermodynamic instabilities in the given environment. It may also be described as the physiochemical interaction between metallic materials and their environment that results in the deterioration of the material.

Monitoring of corrosion is important as it gives insights into the safety and economic use of metals. The cost incurred in replacing corroded structures, prevention of rusting and sustenance of cathodic protection systems for underground pipes can be regarded as direct losses that arise as a result of corrosion. Other direct losses attributed to corrosion include the cost of repainting structures and replacement of water heating systems that fail due to corrosion.

2.3 Effects of Corrosion

There are consequences of corrosion which affect the safety, efficiency and reliability of structures. Other effect relate to the loss of mass of metal which lead to incurrence of maintenance and replacement costs (Gyeongcheol Choe et al., 2020).

Some of these consequences are listed below (El Maaddawy & Soudki, 2007):

1. Loss of mechanical strength of structures that may lead to failure or breakdown due to the corrosion leads to reduced thickness of metals.
2. Failure and breakdown may lead to injury to people.
3. Corrosion results in deterioration in appearance
4. Fluids such as bear in pipes and vessels are contaminated with corrosion, which may lead to adverse health complications.

2.4 Process of Corrosion

Iron is the most widely used of all metals, it is however one of the most adversely affected by corrosion. Iron just like most metals are not found in nature in their metallic states. They are obtained from their naturally occurring compounds or ores by expenditure of large amounts of energy. Their metallic state can therefore be considered as being metastable and will thus tend to revert to compounds similar to their original state by losing energy.

Most corrosion reactions are electrochemical in nature, thus, the iron changes into a solution of ferrous ions at the anodic sites. As the iron atoms are oxidized into ions, negatively charged electrons are released and their build up prevent further reaction.

In order to allow the anodic reaction to proceed, the electrons released must be passed to a metal surface where a cathodic reaction can take place. Here, the electrons will be able to react with a reducible component of the electrolyte thus they will be reduced from the metal.

The following are the important electrochemical reactions of iron (Maria Cristina Tanzi, SilviaFare & Gabriele Candiani, 2019):

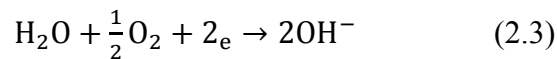
Anodic reaction:



Cathodic reactions:



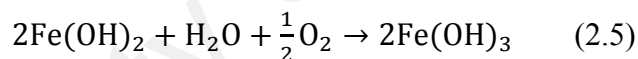
Or



The second reaction (eq. 2.2) is common in acidic environments while the third reaction (eq. 2.3) involves reduction of oxygen and in this case, the corrosion result in formation of solid debris. With further process of corrosion, iron (II) hydroxide, $\text{Fe}(\text{OH})_2$ is produced (eq. 2.4) which the appearance is white in color but due to partial oxidation in air it changes to a greenish color.



Due to further oxidation and hydration, a reddish solid commonly known as hydrated iron (III) oxide, or also known as rust is formed (eq. 2.5). This is a porous precipitate which tends to act as a harmful poultice that results to further corrosion.



2.5 Types of Corrosion

Below are the common types of corrosion seen in industrial field:

2.5.1 General / Uniform Corrosion

This is a type of corrosion that results from direct chemical attack on the metal surface that the metal etches out on the surface, for example by an acid (Almusallam, Al-Gahtani, Aziz, & Rasheeduzzafar, 1996). The figure below shows an example of general corrosion (Al-Sulaimani, Kaleemullah, Basunbul, & Rasheeduzzafar, 1990).



Figure 2.1: Uniform Corrosion (Al-Sulaimani, Kaleemullah, Basunbul, & Rasheeduzzafar, 1990).

Commonly found in ferrous metals, this type of corrosion results in a rusting on the surface of the metal exposed to open air. A typical example of general corrosion is the atmospheric corrosion.

General corrosion results in the removal of the surface evenly hence the name uniform corrosion. Here, oxygen reduction and dissolution of the metal are evenly distributed over the metal surface resulting in the uniform formation of corrosion products (Andrade, Alonso, & Molina, 1993).

2.5.2 Stress Corrosion Cracking (SCC)

This is a type of corrosion caused by the presence of a corrosive environment and at the same time the existence of tensile stresses within a piece of metal (Raul Davalos-Monteiro, 2019). Stresses that can contribute to SCC include the applied, residual and thermal varieties, and also those generated by the build-up of corrosion products during manufacturing (Nishimura & Maeda, 2004).



Figure 2.2: Stress Corrosion Cracking (Nishimura & Maeda, 2004).

It can be seen that this type of corrosion is a combination of both electrochemical and mechanical processes and may lead to an abrupt brittle failure of ductile materials (Rhodes, 2001). Due to the applied stress, a small pit may develop on the metal. This pit may further increase into a crack which exposes a new and active surface which can easily corrode. This leads to further cracking and corrosion a process that will advance quickly until mechanical failure occurs.

This form of corrosion is of great practical importance and represents a permanent risk in numerous industrial installations, in terms of both the economic consequences and the safety considerations involved. It is generally considered to be the most complex of all corrosion types, which need an accurate monitoring tool for the inspection.

The conditions necessary for stress corrosion cracking to occur include (Shoji, Lu, & Peng, 2011):

- Mechanical loading
- A susceptible material
- A highly corrosive environment.

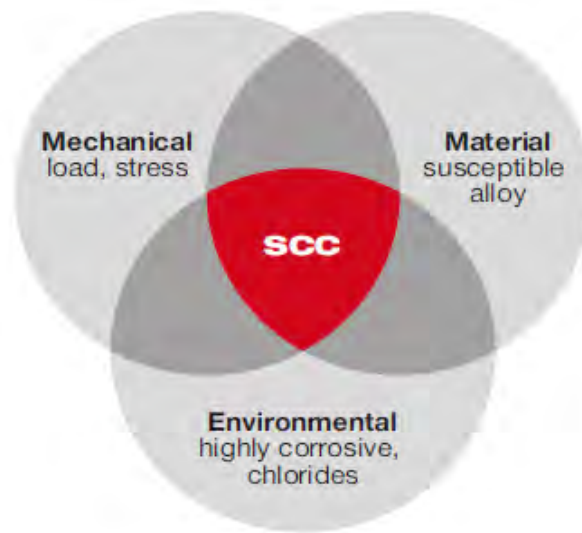


Figure 2.3: Condition for Stress Corrosion Cracking (Shoji et al., 2011).

2.5.3 Corrosion Stress

Corrosion stress can be described as the development of crack formation on a surface usually a metal that is exposed to a corrosive environment. This process may lead to failure of metal structures that are subjected to tensile stress at high temperatures (Rios, Magnin, Noel, & de Bouvier, 1995).

Usually corrosion stress can be difficult to detect as the metal surface may appear shiny and bright yet they are undergoing severe attack from microscopic cracks. This may lead to a sudden failure of structures (Lin, Peng, Lei, Tan, & Shi, 2017). The origin of corrosion stresses can be attributed to crevice loads that result from stress concentration or residual stress from manufacturing and fabrication. The latter can be avoided through various treatment methods like annealing (“Overload Failures,” 2018).

If not monitored, corrosion stress might lead to failure of reinforced concrete. This has prompted the use of various methods to monitor the health of reinforcing bars, one of them being FBG sensors:

2.6 Methods of Corrosion Detection

To provide structural safety, there is need for regular maintenance and constant repairs which should be done on time. This implies that a reliable monitoring method for corrosion of concrete structures is required. The selected method should be able to identify the extent of damage and as a result give an indication of the severity of the problem at any given time (Frangopol & Liu, 2007).

Traditionally, methods that have been used have relied on electrochemistry utilizing techniques such as linear polarization and half-cell potential. However, these methods have short comings as they require physical contact with the concrete structure. Other methods are destructive as they require collection of samples from the structure for analysis to ascertain its health condition. These methods therefore call for scheduled maintenance which is costly and usually they do not provide accurate information on the extent of the damage (A. K. Agrawal, 2001).

Below are some of the traditional corrosion inspection methods that are used in industry for structural health monitoring.

Polarization: is an electrochemical method for corrosion sensing which, just like any other electrochemical method, provides fast and reliable results on the health status of a reinforced concrete structure by inter-relating the chemical and electrical effects on the concrete structure. This is done by measuring the potential and current of oxidation and reduction reactions (Koleva, Wit, Breugel, & Lodhi, 2007).

However, Polarization method comes with several disadvantages; the assumption that the corrosion occurs uniformly leads to misleading conclusions since pitting are most probably form of corrosion in steel and it is rarely uniform (Broomfield, Rodriguez, Ortega, & AM, 1994). On the other hand, this method also depend on the

area of steel measured in concrete which cannot be determined precisely, and this may lead to errors in calculations.

Weight Loss Measurement/ Coupon Test: This is presumably the oldest method for detecting the corrosion of a material in a given environment. The method entails subjecting a specimen (coupon) of the given material to the environment for a specified duration and then measuring the weight loss (Mamoona Zaheer & Muhammad Shahid, 2019). This method of corrosion detection is versatile in nature as the coupons can be made from available alloys (“AIE | Introduction to Corrosion Coupons,” n.d.).

To measure the extend of corrosion, the coupon is exposed to the environment for a specified period and then removed for analysis to be carried out. Basically, this involves calculating the weight loss and deriving the rate of corrosion.

Corrosion rate can be calculated by the equation below:

$$CR = \frac{kW}{DAT} \quad (2.6)$$

Where;

$$k = 8.76 \times 10^4$$

W = Mass loss

D = Density

A = Area

T = Time

This method of corrosion detection is not very instrumental as it requires a lot of manual interaction to collect the information.

2.7 Optical Fiber

Fiber optics as the transmission medium in telecommunication network are recognized by its almost infinite bandwidth, low loss, light weight, immune to electromagnetic interference, transmission security etc. In recent decades, fiber optics had been utilized in the development of sensors in various applications due to its advantages and sensitivity to the measurands (John X.J.Zhang & KazunoriHoshino, 2019).

2.8 Optical Fiber Sensors

Fiber optic sensors are used to detect all signals that change the way light travels or the way light changes as they travel through the fiber. Fiber optics technology has been developed overtime to be used reliably in sensing various parameters such as pressure, strain and temperature in rugged and harsh environmental conditions. These types of sensors are designed to modulate some special characteristics of light such as intensity or phase according to the measurand.

These sensors have the advantage of being small in size, immune to electromagnetic interference, high sensitivity and the ability to be used in rugged environments. They also have a large bandwidth and perform well in high temperature environments.

The fiber optic sensors find wide applications in monitoring because of the many advantages over the traditional electronic sensors. These include (Geib & Singh, 2003):

1. Fiber optic sensors can be easily integrated in structures such as composite material due to their small size.
2. The sensors are immune to electromagnetic and radio frequency interference.
3. These sensors are light in weight.
4. Fiber optic sensors have a high sensitivity.

5. They can be easily multiplexed to form a network of sensors.
6. The sensors are resistant to harsh environmental conditions.
7. They can be used for remote sensing applications.
8. The sensors have multi sensing capabilities and can be used for sensing pressure, temperature, strain and corrosion.

A typical fiber optic system consists of an optical source which may be made of an LED, a laser or a laser diode. It also includes an optical fiber cable and a transducer which converts the measurand into an optical signal (Culshaw, Building, Street, & G, 2004).

The system also includes an optical detector and electronic circuitry such as optical spectrum analyzer which converts the optical signal into electronic form.

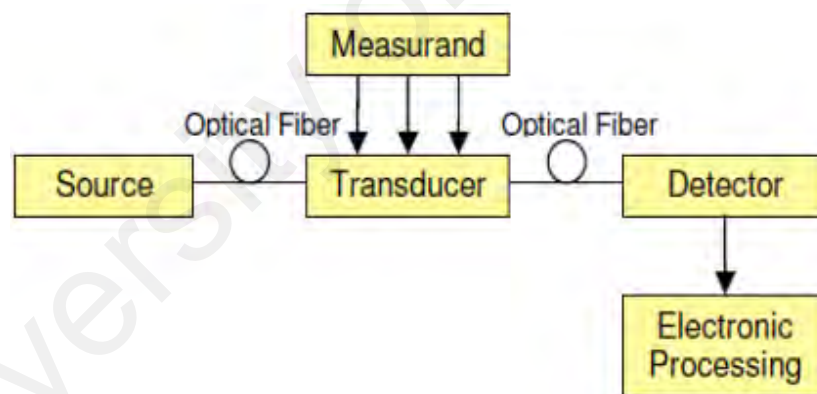


Figure 2.4: Components of an Optical Fiber Sensor System (Muhammad Younus, Pankaj Chakrabarty & Mosharrafa Ahmad, 2015).

Fiber optic sensors have a wide range of applications but most commonly in the following areas:

1. Real time monitoring of the physical health of structures (Antunes, Varum, & André, 2011).

2. Measurement of physical characteristics such as pressure, strain, displacement and acceleration (Hao, 2016).
3. Monitoring of concrete during bridge construction for cracks, pre-stressing, neutral axis evolution and spatial displacement (Measures, 2001).
4. Monitoring of multipoint optical extensometer convergence during tunnel construction (Gong et al., 2019).
5. Monitoring of leakage, foundation, distributed temperature and spatial displacement during dam construction (Schenato, 2017).

2.8.1 Discrete Fiber Sensor

Discrete fiber sensor is a multisensory system composing of arranging a set of discrete sensors in an array configuration and having the individual outputs of the sensors multiplexed. The most common techniques that are utilized in the discrete sensors include spatial multiplexing, time, polarization and frequency. The sensitivity parameters that usually used included optical spectrum, light intensity and polarization. This is because of it can be modulated by parameter such as temperature, pressure, stress, vibration and many more.

Over the past centuries, discrete fiber sensing applications have had increased acceptance in most parts of the world. Mechanical reliability and high optical sensitivity discrete sensor are essential to guarantee reliable performance of fiber optic sensors. Sensor networks such as the device net were developed as a sensor network for small discrete sensors. Discrete leak detection system employs sets of discrete sensors such as Fabry-Perot FBG sensors, to sensor targeted spill-physical attribute. The collections of the discrete sensors are placed as a set of sensors or singly at intervals along the pipeline to be linked by the wireless networks.

Time-division multiplexing (TDM) utilizes a pulsed light source and launches the light into an optical fiber while analyzing the time delay to discriminate between the sensors. Wavelength division multiplexing (WDM) is among the best techniques of discrete multiplexing signal as it employs optical power most efficiently (Huang, Wu, Wang, Wang, & Liu, 2018).

Discrete fiber sensors are used in many industries and markets. The most common application includes part feature verification, machine position verification and part position verification (Z. Ye, Wang, Wang, & Jia, 2016). In machine verification, the proximity of the sensor is used to sense the position of the section of the machine itself.

2.8.2 Distributed Fiber Sensor

Distributed fiber sensors utilize the fiber itself as a sensor to continue, monitor changes in its environments, as well as offers high spatial and temporal profiling over large surfaces with long lengths. This type of sensor is sensitive at each of every point along its length and it provides direct damage detection which avoiding the use of sophisticated algorithms. However, the limitation of distributed fiber optic is the interpretation of measurements is not straight forward compared traditional strain sensors. As the distributed sensor cable is continuous, thus it only provides one dimensional strain field monitoring.

Distributed sensing solutions allow a continuous distributed measurement along the length of the sensing fiber and with this sensor at many locations just with one distributed fiber optic sensor (Bao & Chen, 2012). Distributed fiber sensors provide solutions for reliable and improved as well as affordable monitoring in complicated and broad structures.

The important principles of operation of the distributed fiber sensors can be categorized into three. These principles include the Raman scattering effect, Rayleigh scattering effect and Brillouin scattering effect. Each of these working principles is based on the relationship between the encoding parameter and the measured parameters.

Rayleigh scattering effect is on the shifts embodied in the local Rayleigh backscatter pattern that is dependent on the strain temperature. This enables the strain measures to be compensated for temperature. The main characteristics for this system include high resolution of the monitored parameters as well as short spatial resolution (Zaghloul et al., 2017). Raman scattering effect is based on the non-linear interaction between light travelling through fiber. When the high-intensity signal is directed into the fiber, two-frequency shifted components referred to as Raman anti-strokes (Yan et al., 2019). Brillouin scattering takes place when light that is transmitted by a transparent carrier interacts with the time and space periodic of the carrier vibrations in the refractive index (Yoon, Song, Kim, & Kim, 2011).

Distributed fiber sensors are applied in many industries worldwide. These industries include infrastructure, oil and gas wells, process control, pipelines, homeland security, wind energy turbines, shipboard monitoring, geothermal, military and avionic.

2.9 Fiber Bragg Grating (FBG) Sensor

FBG sensors are attractive sensing devices for Non-Destructive Testing (NDT) (Méndez & Csipkes, 2012) mainly due to its simplicity and a strong reflected signal. These sensors are created by periodically modulating the refractive index of refraction of the core longitudinally. Although there are a large number of ways to use optical fibers for sensing, perhaps the most promising technique involves the use of fiber Bragg grating (FBG).

FBG sensors are characterized by their small size, light weight, immunity to electromagnetic interference and resistance to corrosion (Paulo Roriz, Susana Silva, Orlando Frazao & Susana Novais, 2020). Because of these advantages, FBG sensors are popular in the monitoring of concrete structures (Guo, Xiao, Mrad, & Yao, 2011).

2.10 Principle of operation

Fiber Bragg grating is a grating operates effectively due to a periodic perturbation of the refractive index along the fiber length as shown in Figure 2.5 (Pereira, 2016). When light introduced in a fiber impinges upon the fiber gratings, there is constructive interference between the forward travelling wave and the resulting contra-propagating wave. This interference leads to a narrowband back-reflection of the light signal if the phase match condition (Bragg condition) is met. FBG is written in high Germania Boron co-doped single mode fiber using a phase mask technique.

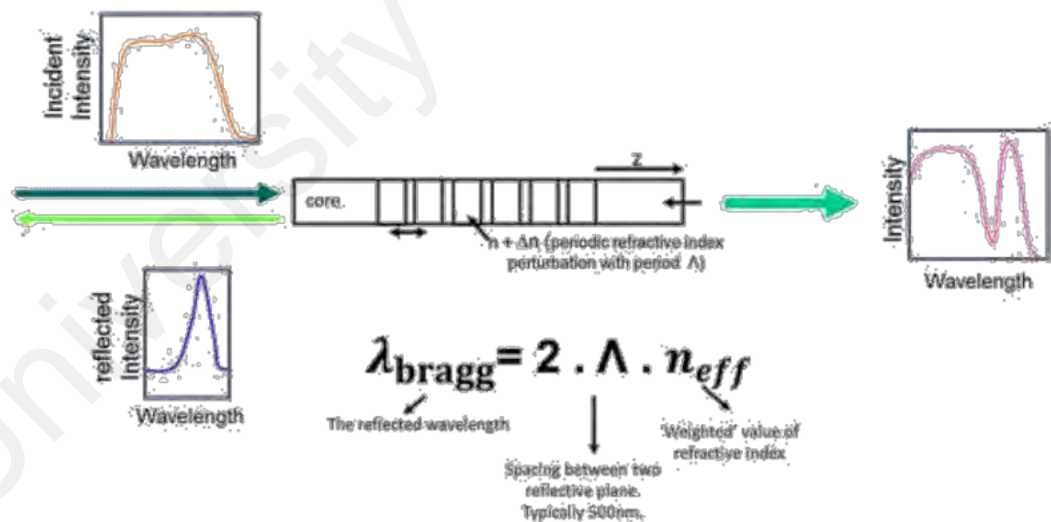


Figure 2.5: An optical fiber Bragg grating structure illuminated by broadband light (Pereira, 2016).

Due to the basic sensing principle used in FBG sensors, the system can therefore be used intrinsically as any local change in temperature or strain results in a change in the

index of core refraction and reflected light wavelength (Himour, Abderrahmane, Beliardouh, Zahzouh, & Ghers, 2005).

In these sensors, the change in wavelength is usually detected by an interrogator which consists of narrowband filters that can be tuned, spectrometers and filters. A unique feature about FBG sensors is that gratings which have different periods can be arranged along the length of one fiber so that each of the resulting reflected signals will have its own unique wavelength. This is useful particularly when multiplexing of several sensors using one optical fiber is required.

2.11 Theory and models of FBG

The Bragg Law of X-ray was discovered in 1912 by Lawrence Bragg, a British Physicist. According to this law, Bragg diffraction will occur when an electromagnetic radiation with a wavelength same as the order of atomic spacing magnitude on a crystalline structure. When this occurs, the electromagnetic radiation is scattered in a specular manner and undergoes constructive interference (Cooper, Elster, Jones, & Kelly, n.d.).

Considering a crystalline solid that has lattice planes that are separated by a distance d , the electromagnetic waves will be interfered constructively on the condition that the path length of each wave is equal to an integer multiple of the wavelength as shown in the figure below (Majumder et al., 2008).

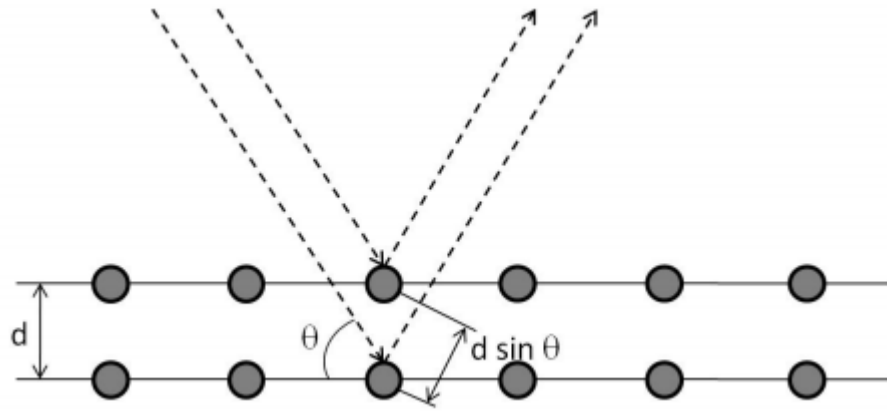


Figure 2.6: Electromagnetic wave interference (Majumder et al., 2008).

An incident radiation is reflected by the lattice structure of a crystal and will interfere constructively if the Bragg law is obeyed. Bragg Law therefore describes the condition to be met for constructive interference to occur from several planes of a crystalline lattice that are separated by a distance d :

$$2d \sin\theta = n\lambda \quad (2.7)$$

Where θ is the incident angle, n is an integer and λ is the wavelength.

To obtain the diffraction pattern, the intensity of the scattered radiation is measured as a function of the incident angle θ . When the Bragg condition is met; it is observed that there is strong intensity in the diffraction pattern referred to as Bragg Peak (Leng & Asundi, 2003).

From the equation 2.7 given that $\theta = 90^\circ$ and d the distance between the peaks of the interference patterns, then for $n=1$, $\lambda=2d$ is the approximated wavelength of the reflection peak. This implies that the optic fiber now acts as a dichroic mirror thus reflecting a portion of the incoming spectrum. For silica, equation 2.7 has to be modified as it was developed for a vacuum. This is because the index of refraction of a given medium affects the distance travelled by light.

$$\lambda_B = 2\eta_{eff}\Lambda \quad (2.8)$$

This implies that the Bragg wavelength of an FBG depends on the effective refractive index (η_{eff}) and the grating period (Λ).

Equation 2.8 is referred to as the Bragg reflection wavelength and is the peak wavelength of the narrowband spectral component that is reflected. The bandwidth of this reflected component also known as the Full-Width-Half-Maximum (FWHM) and is dependent on several parameters but most importantly the grating length. The figure below shows a typical Bragg reflection peak (Majumder et al., 2008).

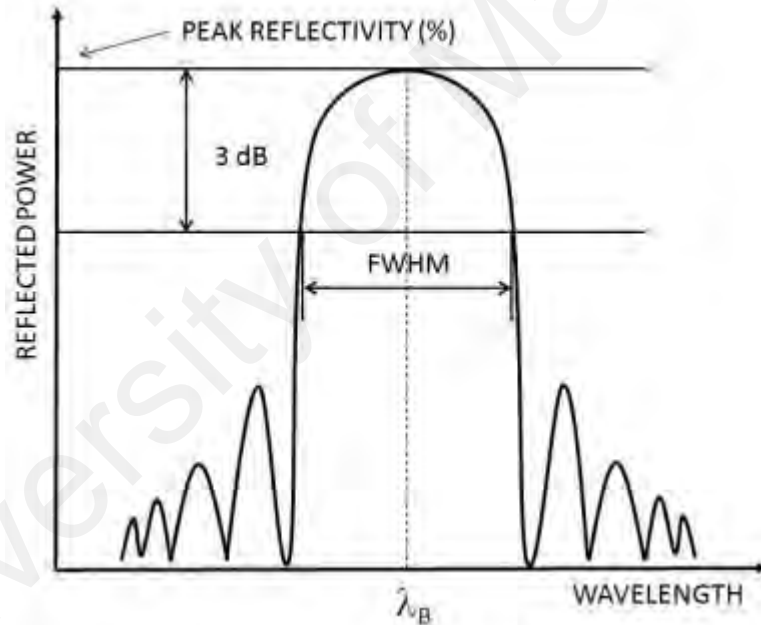


Figure 2.7: Bragg reflection wave shape (Majumder et al., 2008).

We can observe from equation 2.8 that the Bragg wavelength is a function of distance between the gratings (Λ) and the effective refractive index (η_{eff}). An external agent capable of changing the distance between the gratings will as a result be able to displace the reflected spectrum (Chan et al., 2006).

From equation 2.8, it is possible to calculate the sensitivity of the Bragg wavelength with strain and temperature (J.S.Carlton FREng, 2019). The overall effect results in the classical version of the Bragg wavelength sensitivity with strain and temperature as shown below:

$$\frac{\Delta\lambda_B}{\lambda_B} = (1 - p_e)\varepsilon_z + (\alpha + \eta)\Delta T \quad (2.9)$$

Where ε_z represents the grating longitudinal strain.

For a germanium doped core:

$$p_e = 0.22$$

$$\alpha = 0.55 \times 10^{-6} / ^\circ\text{C}$$

$$\eta = 8.6 \times 10^{-6} / ^\circ\text{C}$$

2.12 Advantages of FBG Sensors over Conventional Sensors

The Table 2.1 below outlines the advantages of using FBG sensor for corrosion monitoring and inspection as compared with conventional sensing methods:

Table 2.1: Advantages of FBG Sensors.

FBG Sensors	Traditional Sensors
1. Immune to electromagnetic interference.	Susceptible to electromagnetic interference
2. Can be used in highly corrosive environment	The use in chemically aggressive environment is limited.
3. Light and flexible and can be therefore be embedded in structures easily.	Bulky and rigid and cannot be embedded in structures easily.
4. Allow for easy multiplexing	The multiplexing requires formation of complex networks.
5. Are durable when subjected to high strain.	Due to their construction, they are delicate in nature.

6. Can be used in extremely high and low temperature conditions.	The use is limited by adverse temperature conditions.
7. Do not require electric energy at the sensing location.	Require electric energy at the sensing location.
8. More sensitive as compared to conventional sensors.	Less sensitive as compared to FBG sensors.

From the above comparison, FBG sensor have more advantages and able to use in different field of applications as compared to the traditional sensors especially on the non-destructive and higher sensitivity.

2.13 Polydimethylsiloxane (PDMS)

PDMS is an organosilicon compound that contains a Si-O bond in one molecule. This group of compounds often known as silicon rubbers and is characterized by low toughness but remains unchanged in a wide range of temperatures. This group of silicon rubbers can be categorized into: phenyl substituents for improved flexibility in low temperature, trifluoro-propyl substituents for oil and fuel resistance and for general use.

PDMS is also a low cost material and it has very good optical and mechanical properties as well as low shrinkage and it can be fabricated very easily. Its refractive index is around 1.41 (Vaclav Prajzler et.al., 2020) and it is highly transparent to a wide range of wavelengths (Christos Markos, Kyriakos Vlachos & George Kakarantzas, 2012).

From its chemical composition, PDMS is an optically transparent material that contains a very small amount of impurities. This implies that this material is not an appropriate living environment for bacteria. Furthermore, it is chemically stable and works well in harsh environment with high temperature up to 300 ° C and UV resistant (Cheung, Toda-Peters, & Shen, 2012).

PDMS also finds other applications in automotive industry, electronics and astronautics. This material is produced from hydrochloric acid, methanol and technical silicon a combination that result into chloromethane. During this production, there are four phases namely: synthesis, rectification, hydrolysis and poly-condensation (Rahim et al., 2009) (Yeo et al., 2005).

After these processes, a final chemical composition known as PDMS is obtained and can be shown below:

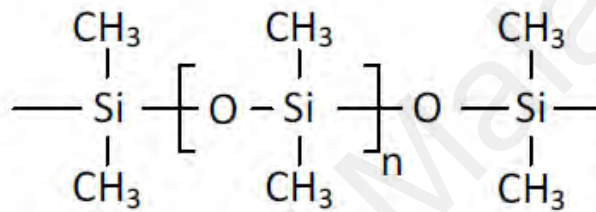


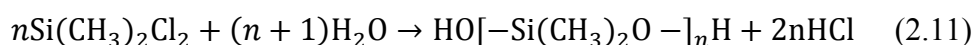
Figure 2.8: Chemical composition of PDMS (Zhongde Dai, Luca Ansaloni & Liyuan Deng, 2016).

PDMS are also characterized by a high Poisson's ratio, low Young's Modulus and high thermal coefficient among other mechanical properties. The chemical formula for PDMS is given by:



Where n denotes the number of monomers present repeating in $[\text{SiO}(\text{CH}_3)_2]$ units.

In industrial manufacturing, PDMS are made using water and dimethyldichlorosilane. The chemical reaction for this process is given below (Wu et al., 2000).



During this process, hydrochloric acid is emitted during polymerization. Due to the challenges posed when handling this acid, a better process has been developed to be used for domestic and medical purposes. In this process, the chlorine atoms are replaced with acetate groups and thus the polymerization process will produce acetate acid which is not chemically aggressive as HCl (Sawpan, Pickering, & Fernyhough, 2011).

The following are some special properties of PDMS that make them popular in various applications (Gallardo & Román, 1993):

1. Resistance to UV radiation
2. High permeability to gases
3. Minimal temperature effect
4. Thermal stability
5. Excellent surface activity
6. Physiological Hydrophobic inertness.
7. High volatility at low molecular weight.

Due to its unique characteristics such as a large thermo-optic coefficient, low Young's modulus and a high Poisson's ratio, the PDMS coating is very suitable as a transducer for temperature and transverse load.

Generally, with increasing pressure the PDMS will increase the expansion and reduce refractive index on the surface of the fiber. This consequently increases the sensitivity of the sensor (Handawi, Vahdati, Shirayev, & Lawand, 2017).

2.14 pH Sensitive Hydrogel

One of the main challenges experienced by concrete structures is the occurrence of cracks which is a result of the low tensile strength of concrete. Occurrences of these

cracks allow entrance of harmful substances dissolved in fluids and gases which compromise the durability of the structure (Osada & Ross-Murphy, 1993).

Once the cracking has occurred, high costs are incurred in manual inspection of the structure. However, the manual inspection cost can be reduced by using a special polymer coated FBG as non-destructive monitoring of the structure. This polymer is usually a hydrogel. The working of this hydrogel depends upon the changes in pH, which helps to increase the sensitivity for corrosion detection without destructing the building structure. The hydrogel can also be described as a cross-linked polymer network which is capable to swollen with pH (Parhi, 2017).

This is due to the presence of these side groups which have a charge that is dependent on pH. When these side groups become charged, additional counter-ions must be present to ensure that the hydrogel remains electrically neutral. However, presence of additional counter-ions results in a difference osmotic pressure between the solution and the hydrogel, and this will consequently result in the gel taking up the solvent and swelling until the elastic forces within the gel are at equilibrium with the osmotic forces (Kim & Peppas, 2002).

Figure 2.9 shows the structure of hydrogel. Consider a hydrogel that with acidic groups bounded to its polymeric chain. When in acidic conditions, the hydrogen ions will come off and combine the hydroxide ions to form water molecules. As a result, for the charge neutrality to be maintained there must be charge compensation by cations which will enter the hydrogel alongside the hydroxide ions (Serpe, Jones, & Lyon, 2003).

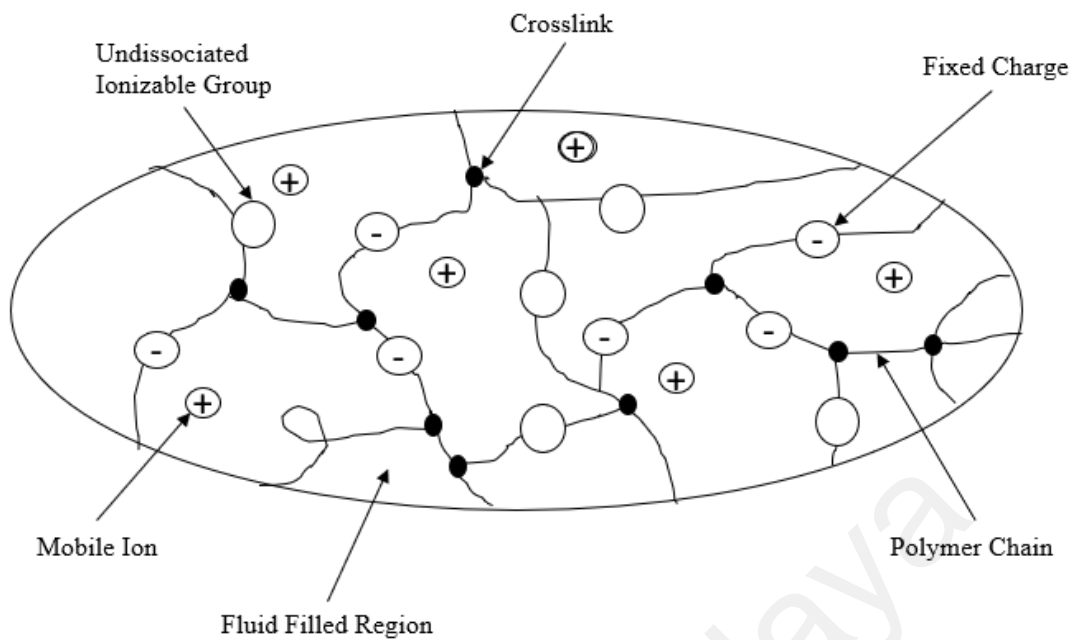


Figure 2.9: Structure of hydrogel (Mahdavinia et al., 2004).

This increased concentration of cations will result in the rise of osmotic pressure causing the gel to swell or de-swell as shown in Figure 2.10 (Mahdavinia et al., 2004).

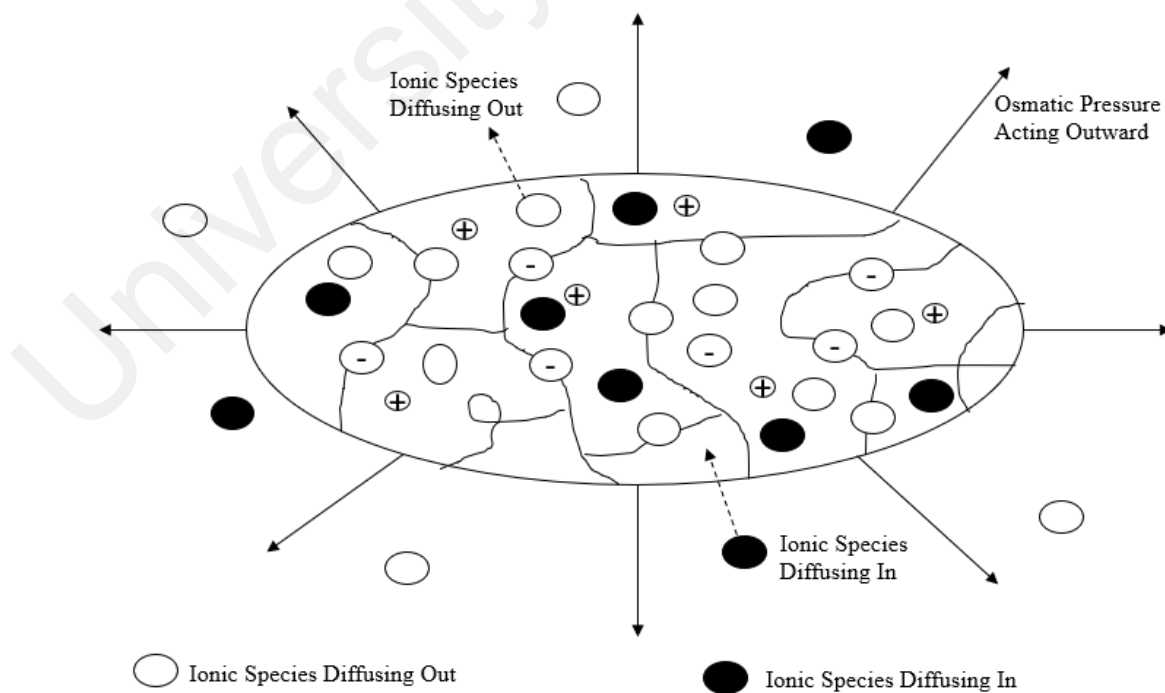


Figure 2.10: Swelling phenomena of a hydrogel (Mahdavinia et al., 2004).

This expansion will not continue indefinitely as the physically cross-linked network of the polymer will counter balance the stretching to prevent destruction. The net force resulting from this balance is known as the swelling pressure (P_{sw}) which is zero at equilibrium. In another word, equilibrium is achieved when the osmotic forces balances the elastic force of the network.

Due to the unique swelling characteristic of hydrogel depending on pH value, thus, hydrogel can increase the sensitivity of corrosion detection.

2.2 Summary

This chapter has described the impact of corrosion to the structural building and the importance of early corrosion detection. Various corrosion types and conventional method of corrosion detection are as well reviewed. As this research work is focus on the development of FBG as early corrosion detection; hence the operation of FBG and the advantages over the conventional method is discussed. Final discussion on this chapter focuses on the fundamental of PDMS and hydrogel as FBG coating material.

CHAPTER 3: RESEARCH METHODOLOGY

3.1 Introduction

This chapter discusses the characterization methods to develop a sensor for early corrosion detection via FBG sensor. The approach is divided into three parts that includes Bragg grating etching, coating development, characterization, and the application of FBG coating on rebar surface.

The first section shows the general flow chart of the research work that was undertaken to acquire the desired objectives. It then follows by the discussions on etching and characterization of Bragg grating. Section 3.4 and 3.5 focused on the explanation and experimental setup of PDMS and hydrogel coating; while section 3.6 discusses the conventional technique for corrosion measurement.

3.2 Research Methodology Flow Chart

The methodologies of SHM using FBG sensors are illustrated in Figure 3.1, and the method used in this work is mainly based on the shift of FBG wavelength resulted from the sensitivity of the material coating to the FBG sensor.

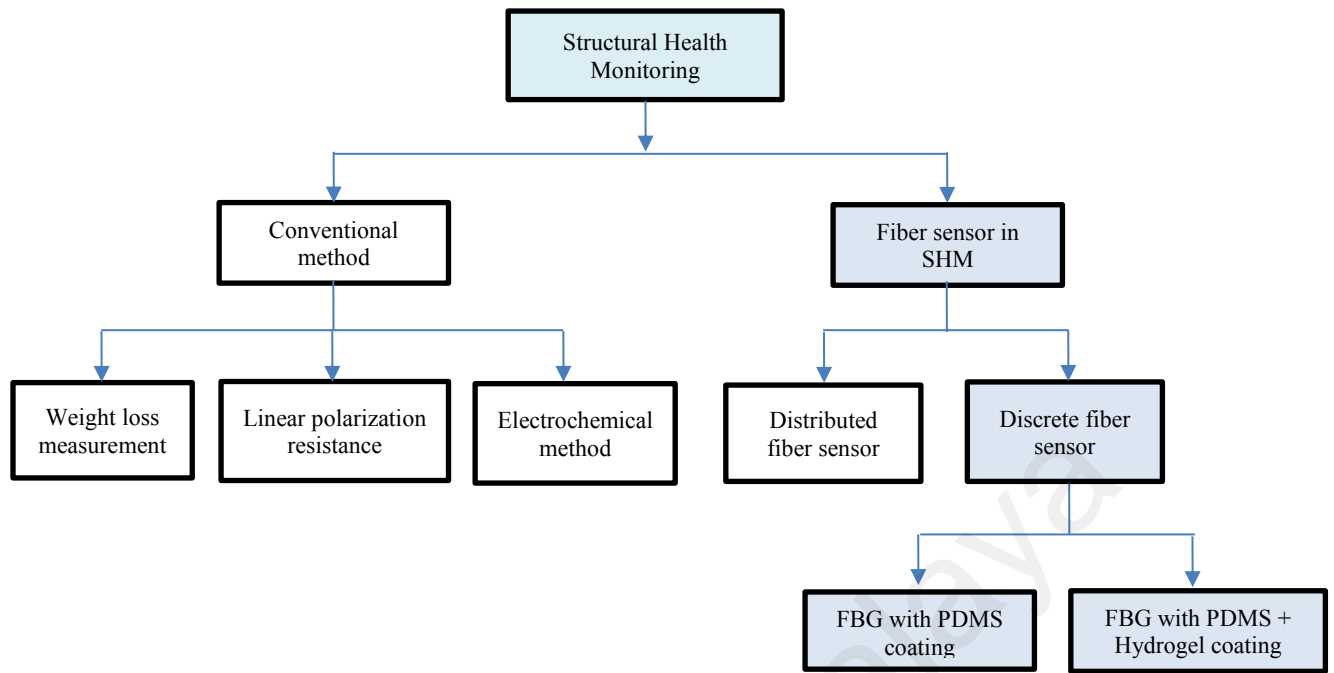


Figure 3.1: Research methodology.

The coating material improves the strain sensitivity and ensures early detection (Mishra, Lohar, & Amphawan, 2016). In this work, PDMS and hydrogel were chosen to be the two main materials to increase the coating sensitivity for early corrosion detection.

The first coating mixture was PDMS with pre-polymer and initiator; while the second coating material was the mixture of PDMS and Hydrogel. A well-mixed coating for the FBG sensor could effectively increase its sensitivity to corrosion detection. This can be achieved by varying the ratio of the mixture until a layer with desired characteristic is obtained. The generated shift in peak wavelength from the corrosion process, which induced strain effect, was evaluated daily.

3.3 FBG Etching

The first work carried out was the FBG etching to improve the sensitivity of the FBG. This can be explained by the effect of the concentration of strain where geometric discontinuities cause the object to experience an increase of intensity in stress field at a localized area (Khechai, Tati, Guerira, Guettala, & Mohite, 2018). Figure 3.2 shows the first part methodology flowchart of the FBG etching process.

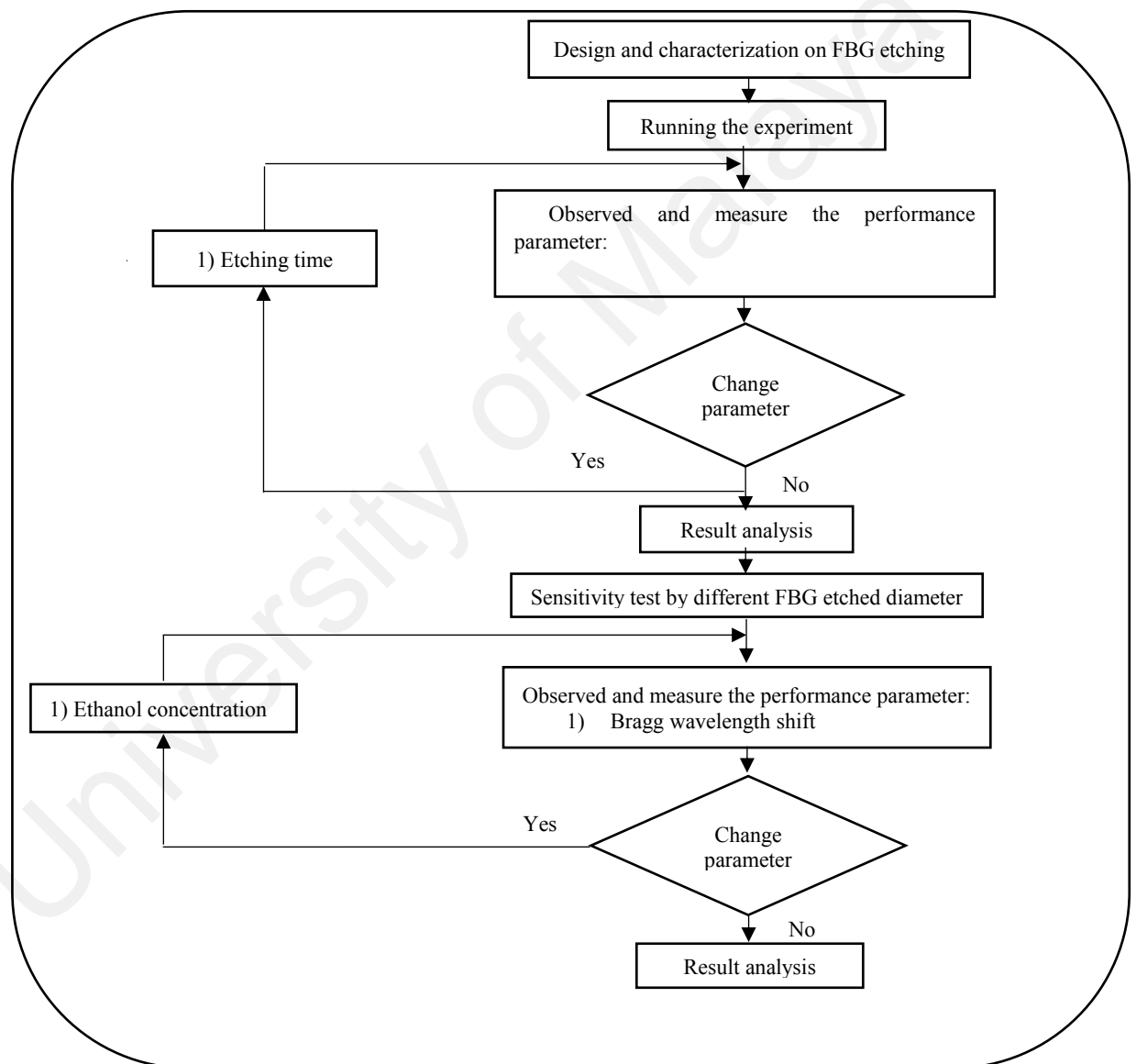


Figure 3.2: Experiment methodology flowchart 1.

The FBGs have a fiber cladding and core diameter of 125 μm and 8 μm respectively. They were dipped into a solution of 49% Hydrofluoric acid (HF) at room temperature. Figure 3.3 shows a broadband signal from an Amplified Spontaneous Emission (ASE) light source is injected into the fiber through a 3-port circulator. During the entire etching process, an Optical Spectrum Analyzer (OSA) was used to monitor the reflected spectra from the FBG.

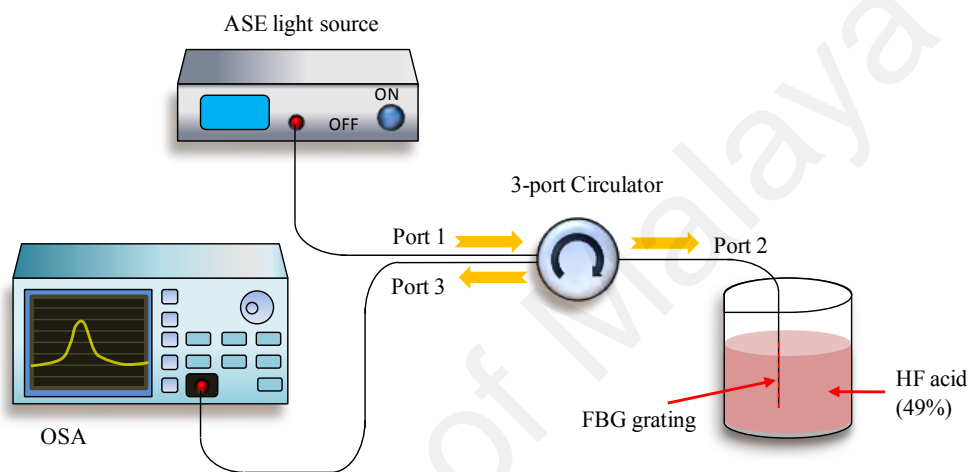


Figure 3.3: FBG etching experiment setup.

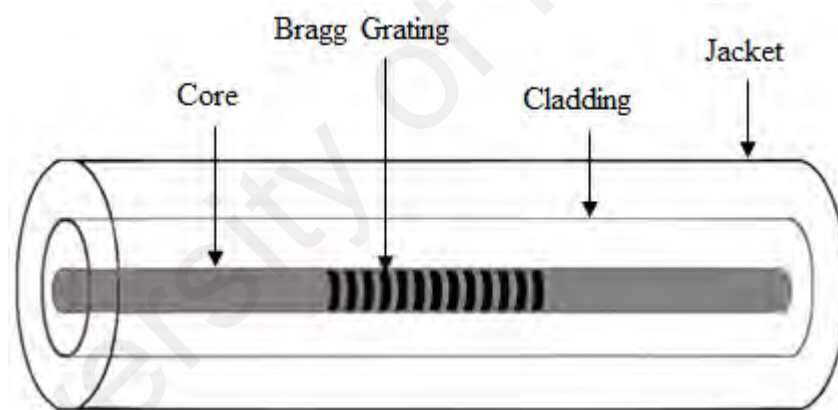
The FBG was immediately rinsed through DI water after etching to remove the remaining HF solution and left to dry prior coating process. The FBG wavelength was recorded at room temperature before and after etching, and the final FBG fiber diameter was then inspected and measured via Scanning Electron Microscopy (SEM).

The total etching duration was approximately 19 minutes and 20 seconds, and as a result, the FBG diameter was etched from 125 μm to 9.7 μm . The FBG was etched near to the core layer to appreciate the sensitivity enhancement due to evanescent sensing. Ethanol concentration test on different FBG diameter was carried out to ensure 9.7 μm will provide the most sensitive in wavelength shift. In addition, A COMSOL simulation

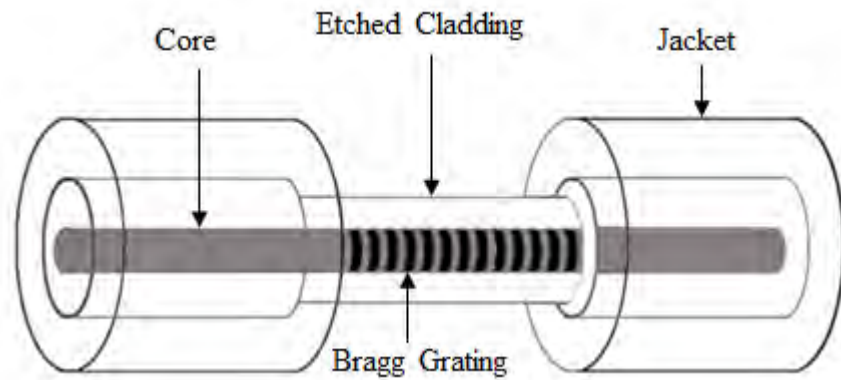
software was also used to model the evanescent exposure for un-etched and 9.7 μm FBG diameter.

Evanescent field is a phenomenon that arises at the interface of two non-absorbing media due to total internal reflection. It occurs when a light beam travels through the first media which has a higher refractive index meets the interface of the second media which has a lower refractive index at an angle which is greater than a critical angle (G. Agrawal, 2013). When this happens the light beam is reflected totally back into the medium with the higher refractive index.

Figure 3.4 shows an illustration of the FBG before and after etching of the Bragg grating, respectively.



(a): FBG before etch.



(b): FBG after etched.

Figure 3.4: FBG before and after etched.

Different FBG diameters were tested through different ethanol concentration, and the ethanol concentration was measured via ATAGO refractometer. Interaction of FBG with different concentrations of ethanol enables the study of sensitivity of FBG with different diameters by observing the peak wavelength shift. Different diameters of FBG produced different fiber evanescent fields when exposed to the environment. It was hypothesized that FBG nearest to the core layer results in a higher exposure of the evanescent field to the environment, thus enhancing sensitivity. This, in turn, produces a greater wavelength shift when interacted with the surrounding environment.

Another factor which is the surrounding temperature needs to be monitored as well, as this effect is considered as noise, which would result in inaccurate results. In this experiment, a temperature compensation equation was used to compensate the effect of temperature on the results.

3.4 FBG with PDMS Coating

PDMS is a silicon-based organic polymer and mostly used in the manufacturing of biomedical sensors and semiconductors because of its strain sensitivity properties

(Luciano et al., 2012). PDMS can be used in either semi-solid or liquid environments due to its cross-linked molecular structure.

PDMS have high molecular weight and allow effective measurement of extreme conditions such as large strain. In addition, it is also an optically transparent material that contains a very small amount of impurities. This implies that this material is not an appropriate environment for bacteria. Furthermore, it is resistant to high temperatures, chemicals, UV radiation, and it is also tasteless and odorless.

A combination of an initiator mixture and pre-polymer was used to fabricate the PDMS coating. Being a cross-linking agent, the initiator mixture helps to strengthen the PDMS solution. The initiator and pre-polymer were mixed at a ratio of 1:10 and was stirred for 5 minutes. Preparation of the solution is shown in Figure 3.5. The resulting mixture was kept at room temperature for 20 minutes so as to displace the trapped air bubbles.

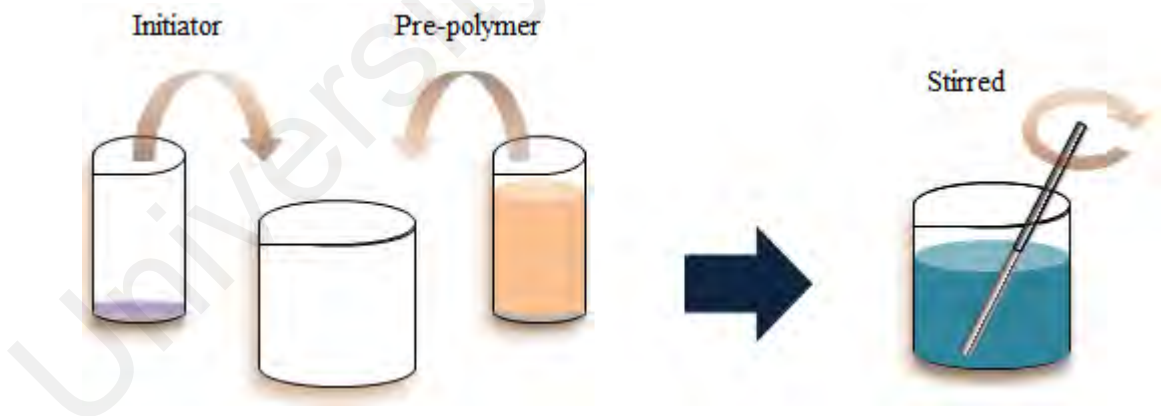


Figure 3.5: PDMS solution preparation.

Several procedures were carried out to study the performance of FBG sensor with PDMS coating. The samples were prepared by pouring a thin layer of PDMS solution into the mid-section of an aluminum plate. The aluminum plates were then kept at room

temperature (25 °C) so as to displace any remaining bubbles. This results in flat surface on the solution on aluminum plate as shown in Figure 3.6 below.

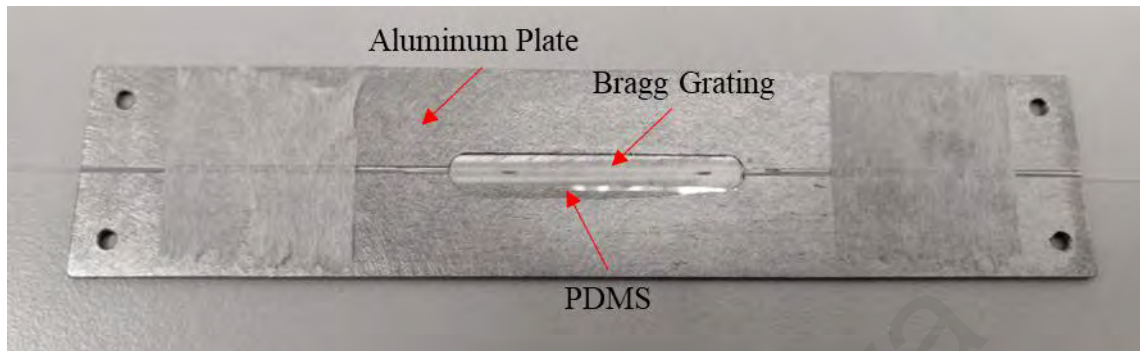


Figure 3.6: PDMS solution on aluminium plate.

A rebar with 30 cm length was then mounted on the aluminum as shown in Figure 3.7. For references purposes, the same was done to an un-coated FBG. Two sets of FBGs were prepared for the characterization of sensors and embedded onto the same rebar. The rebar was then exposed to humid and heat environment to induce corrosion. The Figure 3.8 below is an illustration of the PDMS layer coated on FBG. The overall flowchart is shown in Figure 3.9.

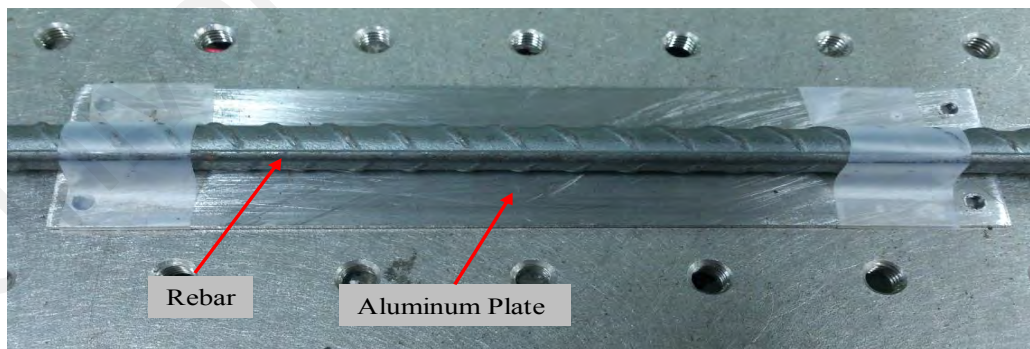


Figure 3.7: Rebar mounted on an aluminum plate.

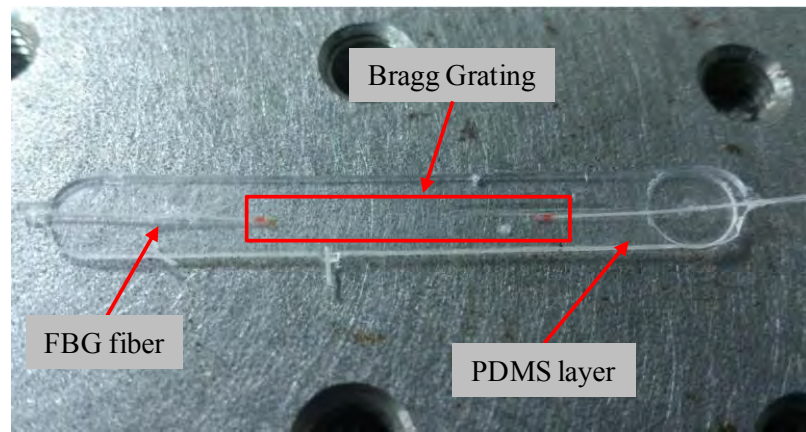


Figure 3.8: A thin PDMS layer coated FBG fiber.

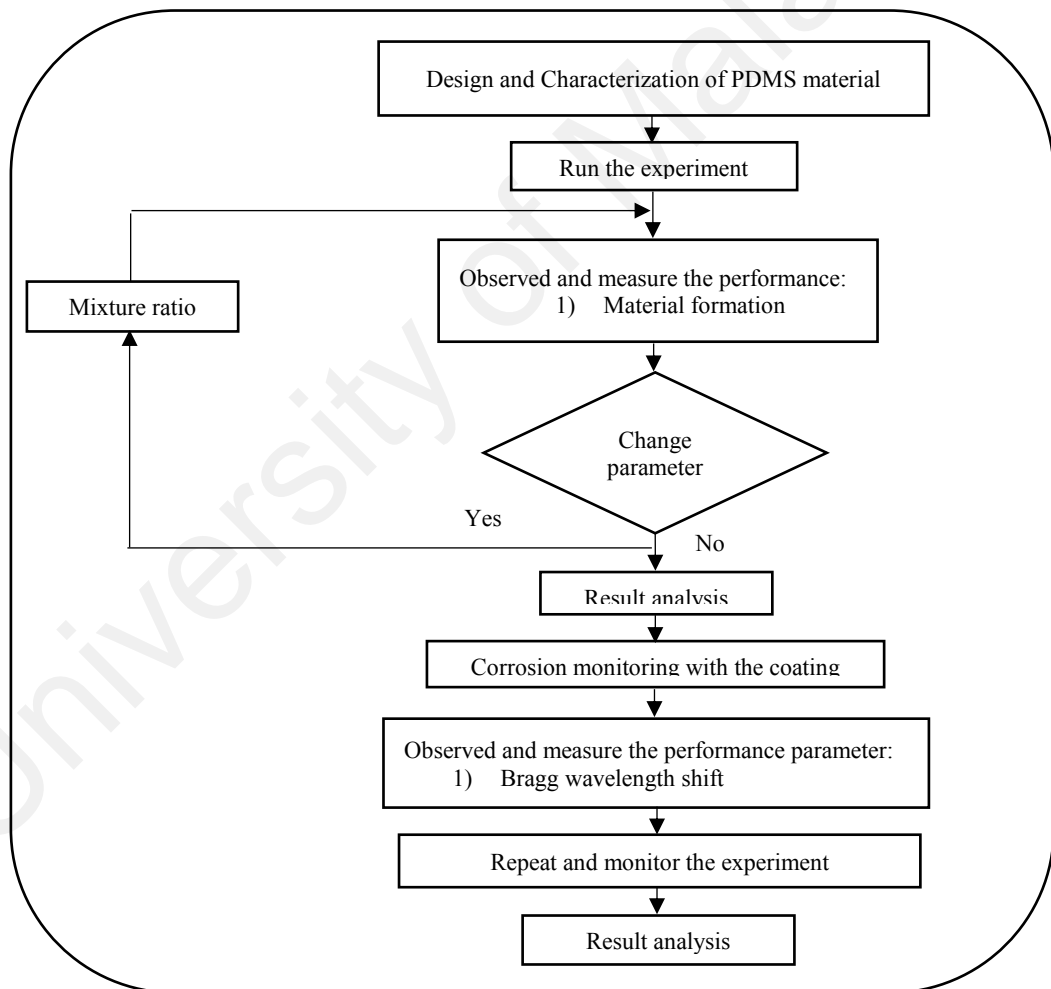


Figure 3.9: Flowchart 2 experimental.

Temperatures were also recorded via digital temperature meter. This way, the effects of temperature on FBG wavelength shifts can be taken into account and compensated. An FBGA was used to monitor the FBG wavelength shifts and the results were recorded and monitored until the rebar corrosion was observed. A total of 30 samples were prepared, monitored and recorded for repeatability data analysis.

3.5 Mixture of PDMS and Hydrogel Coating

Another type of coating material that would help in sensitivity improvement for corrosion process monitoring is the hydrogel materials and PDMS mixture. Different mixing ratios of the two materials were tested to determine the best coating layer for FBG sensor. The mixture will remain in liquid form if they are not mixed in the proper ratio.

Similar with the procedure in section 3.4, a combination of PDMS and hydrogel was used to fabricate the coating. The hydrogel is sensitive to pH changes and swells when in contact with pH; while PDMS is a strain-sensitive material (Kersey et al., 1997). The PDMS initiator and pre-polymer were first mixed; the hydrogel was then added to the solution and stirred for 5 minutes. The ratio of PDMS to hydrogel is 0.15:0.85. The mixture was kept at room temperature for 20 minutes to displace the trapped air bubbles. Preparation of the solution is shown in Figure 3.10; while the overall flowchart for this mixture is the same, as shown in Figure 3.9.

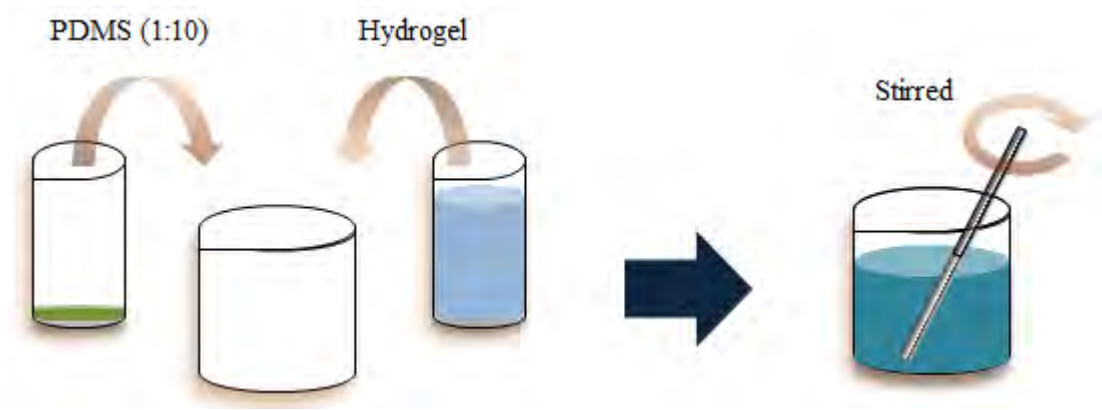


Figure 3.10: PDMS-hydrogel solution preparation.

As mentioned in section 2.14, hydrogel is sensitive to pH conditions, when there is a decrease in pH with the hydrogel coated FBG, the hydrogel will swell and caused the mechanical expansion, thus stretches the FBG and changing the grating period resulted shift in Bragg wavelength (Liu, Zhang, Cong, Xu, & Chen, 2003).

The FBG wavelength shifted more when in contact with an acidic environment as compared to an alkaline environment. The straining effect on the FBG sensor develops when hydrogel swells in contact with acidic pH, results in the wavelength shift. Corroded rust will produce H^+ ions (Chilingar & Mourhatch, 2008), with pH around 4.3, thus it tends to become an acidic condition and induce structural change in the hydrogel (Lutron, pH 222). This characteristic realizes the development of corrosion sensor by hydrogel coated FBG.

The FBG wavelength shift was recorded and monitored until the rebar sample was corroded and the wavelength become constant for a total of 30 samples for repeatability data analysis. The overall setup of the monitoring research works as shown below in Figure 3.11.

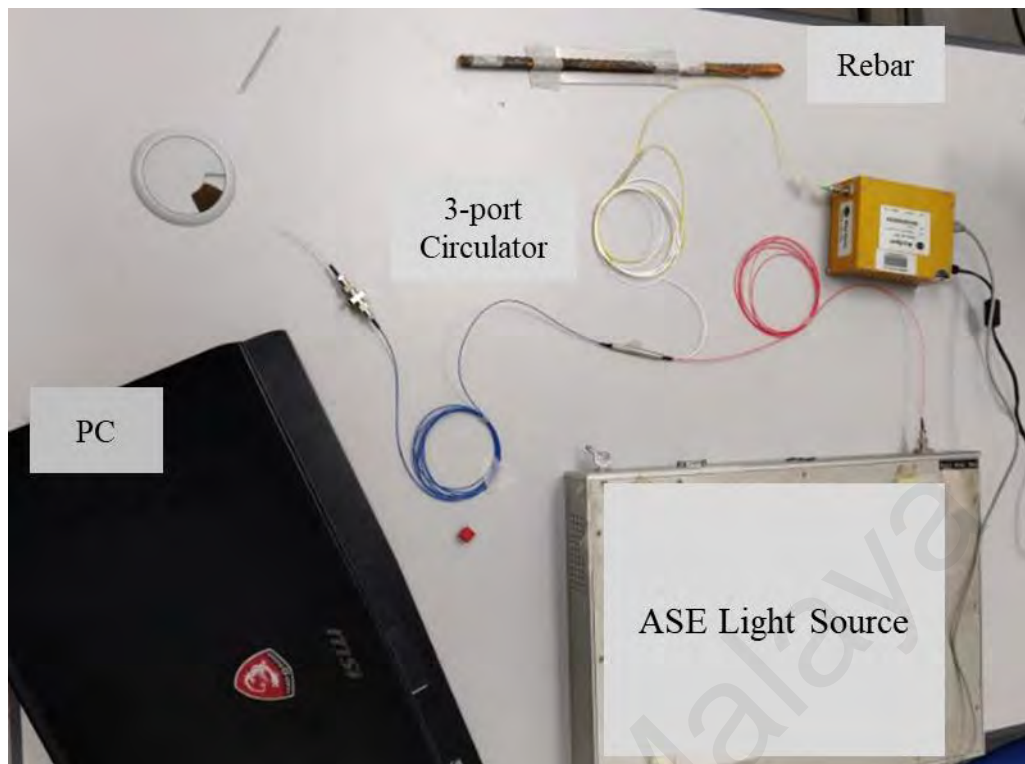


Figure 3.11: Experiment setup.

3.6 Weight Loss Test

Weight loss test is the simplest conventional way for corrosion rate measurement. This is done by exposing the sample to the test medium and time is taken into account when measuring the weight loss.

In this experiment, corrosion rates were calculated and used as a comparison data to FBG wavelength shift. Below are the steps followed in performing weight loss test (ASTM, 2008):

1. Measure the dimension and weight the sample.
2. Exposed the sample to induced corrosion.
3. Prepare a 1000 ml HCl cleaning solution into a beaker based on the ASTM G1 standard.
4. After 24 hours, take out the sample, place the sample into the cleaning solution and place the beaker into the ultrasonic cleaner.

5. Clean the sample for 5 minutes.
6. Wash the sample with DI water and rinse with alcohol to clean the sample.
7. Dry the sample with an air gun blower.
8. Handle test samples with care using gloves and tweezers to avoid contamination of the surface after cleaning.
9. Weigh the clean sample on an analytical balance
10. Record the weight.
11. Repeat step 4 to 10 until the mass loss is not significant. This is to ensure data collection accuracy.
12. Calculation of corrosion rate was discussed in Chapter 2 at eq.6.

3.7 Summary

In this chapter, methodologies adopted for this research work are presented. Design and performance parameters characterizing the etched FBG and FBG coating layer were carried out and discussed. These parameters are used throughout the study to assess the performance of the proposed structures.

CHAPTER 4: RESULTS AND DISCUSSION

4.1 Introduction

In this work, a new coating of FBG sensor for strain and pH sensing has been developed for corrosion detection. This method focuses on developing sensitive coatings around an etched Bragg grating for strain and pH detection.

4.2 FBG Etching

The basic principle of the FBG sensor relies on the change in Bragg resonance wavelength to the effective refractive index, and grating pitch. If the fiber cladding diameter is reduced along the grating region, effective refractive index, η_{eff} is affected by the external refractive index, RI thus increase the FBG sensitivity. In addition, etching can also result in a significant reduction in the force required to induce strain (Lyons & Lee, 1999). The response of a Bragg grating is dictated by the known Bragg equation, as stated in equation 2.8.

FBG was etched using 49% HF acid to reduce the thickness of cladding layer. During the first 18 minutes of the wet chemical etching process, the wavelength depicts a red shift, which is an increment in wavelength. This is because of the heat produced by the chemical exothermic reaction during the entire etching process (Sadrayi, Saffarzadeh, & Boroujerdian, 2019), $\text{SiO}_2 + 4\text{HF} \rightarrow \text{SiF}_4 + 2\text{H}_2\text{O}$ (Yun, Chen, & Cui, 2007), (Zhang, 2013). Since the FBG itself is temperature-sensitive, when the heat is produced and interacts with the Bragg grating, the wavelength shows a red shift, as shown in Figure 4.1 below. However, after 18 minutes of etching, the wavelength starts to show a blue shift until the etching process completed as shown in Figure 4.2. This is

attributed to the changing of n_{eff} , caused by the cladding reduction. Figure 4.3 shows the original wavelength before etching process started, for reference.

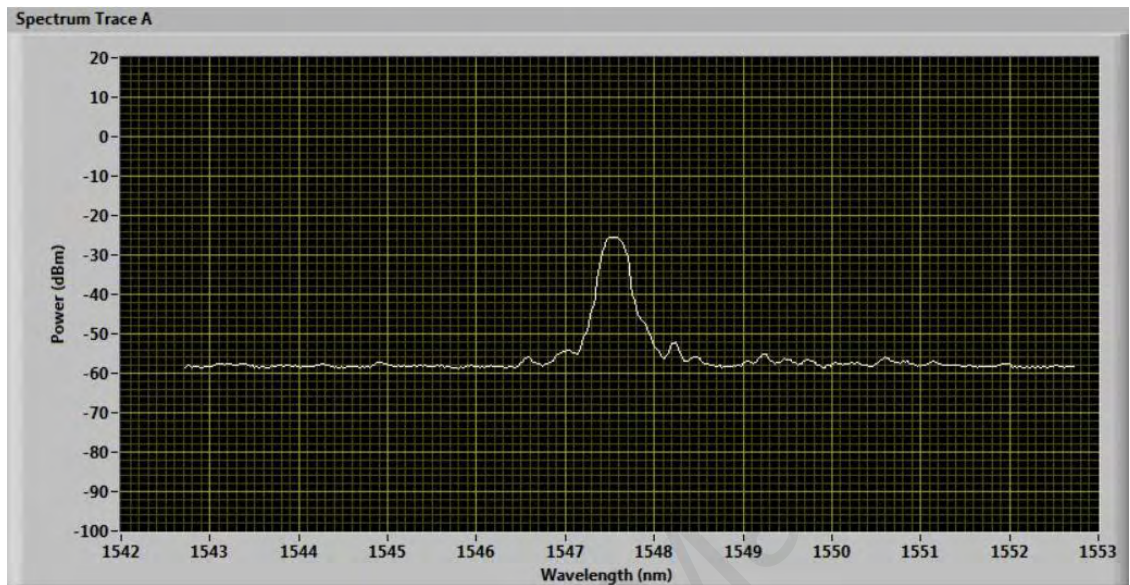


Figure 4.1: FBG wavelength (1547.54 nm) at 18 minutes of etching.

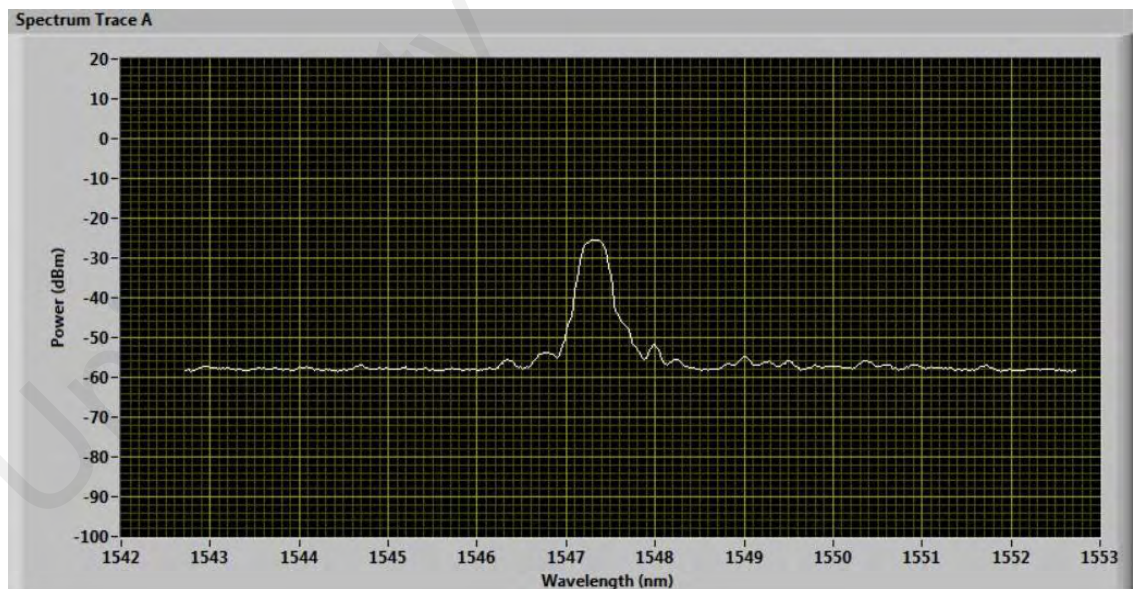


Figure 4.2: FBG wavelength (1547.24 nm) at 19 minutes 10 seconds of etching.

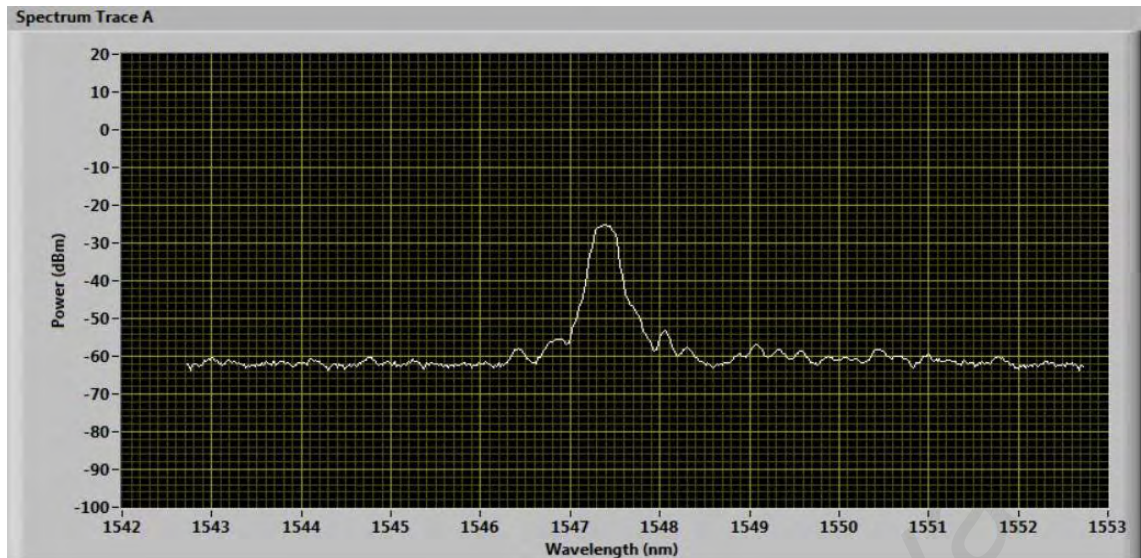


Figure 4.3: FBG wavelength (1547.38 nm) at T0.

Figure 4.4 below shows the FBG diameter by etching time. Error bars are used to depict the standard deviation of the result. FBG were etched with 9 different etching times, and they are repeated 30 times etching to study its repeatability and accuracies. The error bars shown represents the etching variation over etching time with the errors ranging from $0.10\ \mu\text{m}$ to $0.14\ \mu\text{m}$. A small value of error shows that the etching can be controlled precisely and repeatable. The total etching time to obtain $9.7\ \mu\text{m}$ core as close to the fiber core of $8.2\ \mu\text{m}$ diameter was at 19 minutes and 20 seconds.

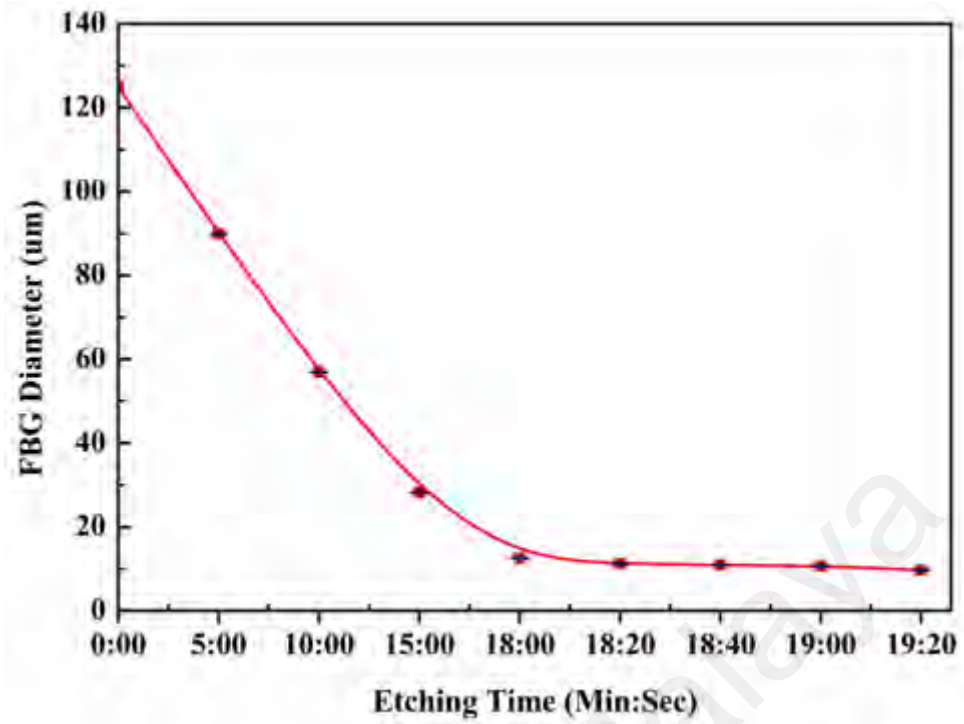
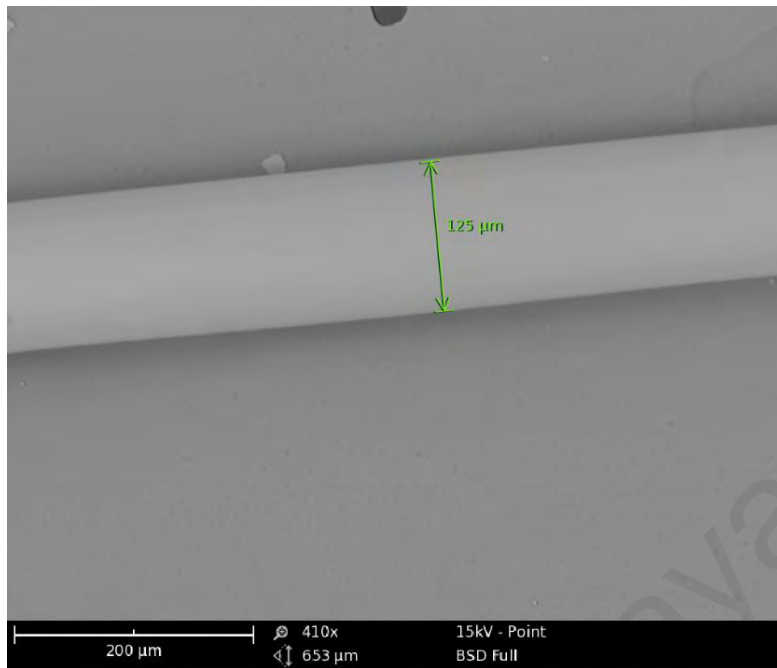
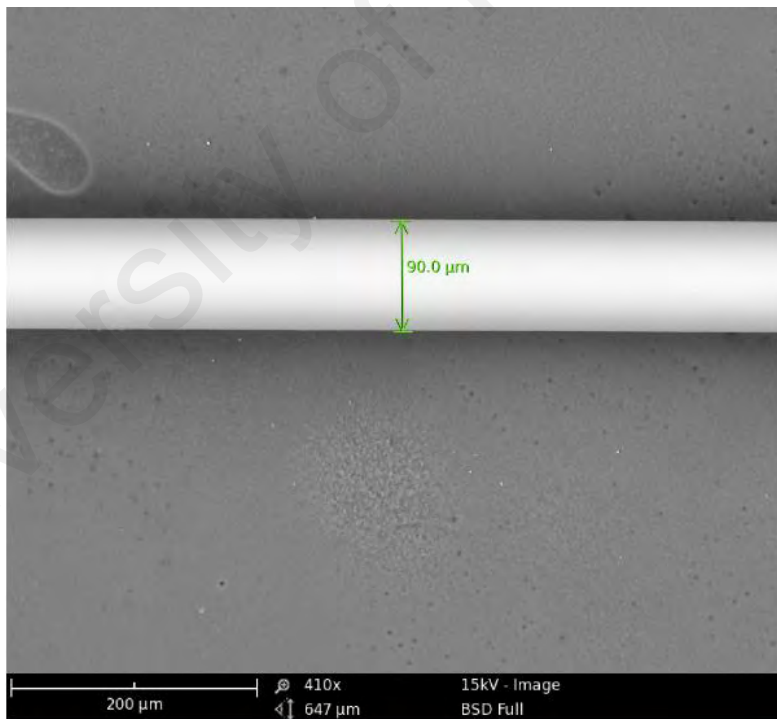


Figure 4.4: FBG diameter by etching time with error bars.

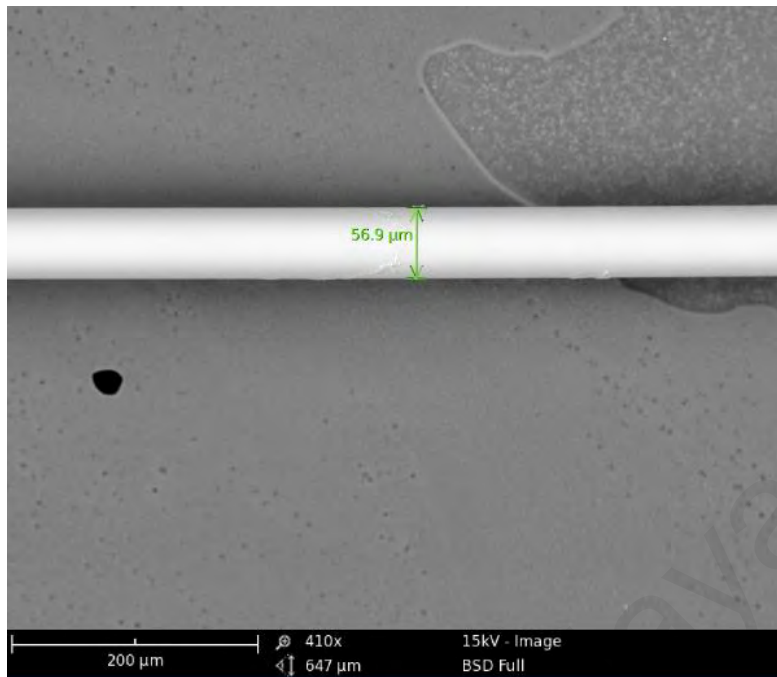
FBG fibers were observed and measured via SEM after each time of the etching to control over-etches of the FBG. Figure 4.5 shows the SEM images for the fibers diameter along etching time under 15kV.



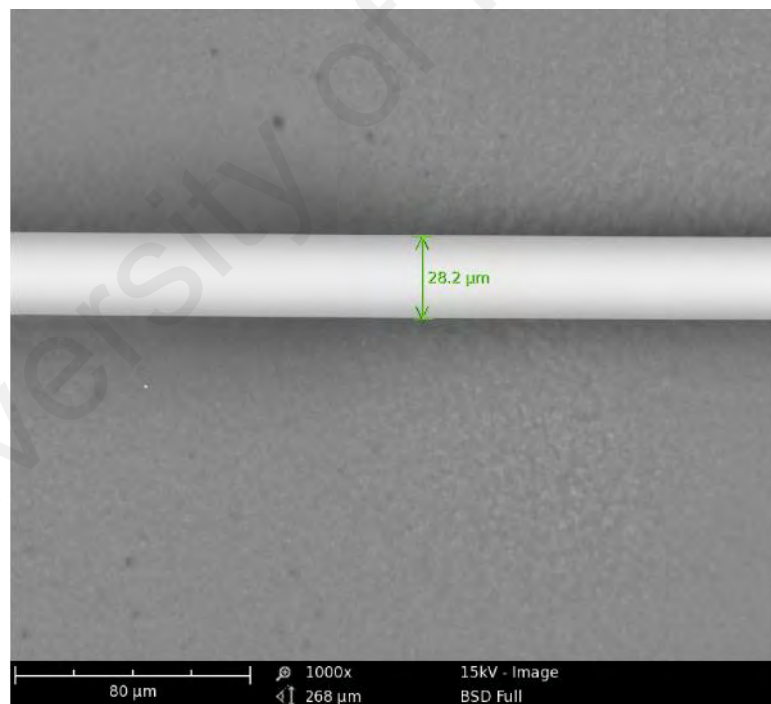
(a): Un-etched 125 μm, under 410x of magnifying.



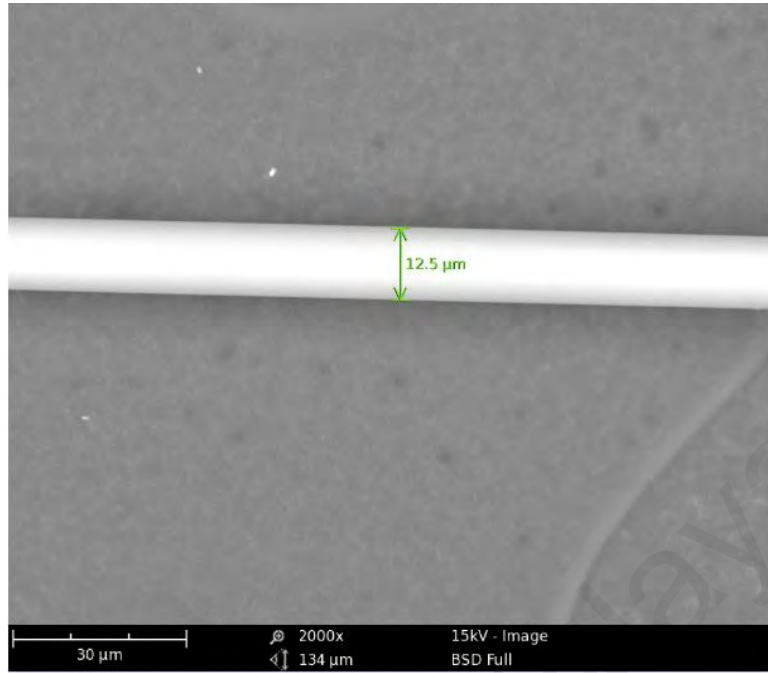
(b): Etched (5 mins): 90 μm, under 410x of magnifying.



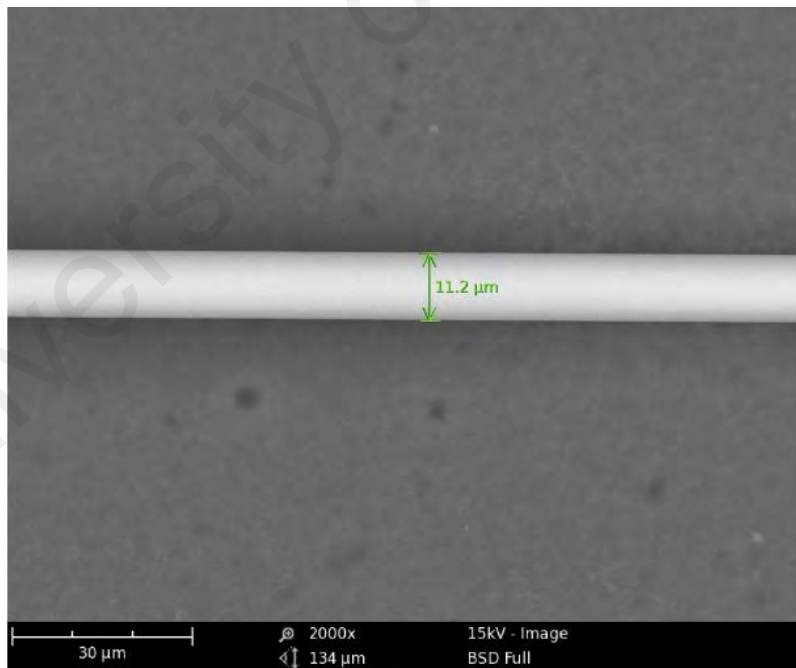
(c): Etched (10 mins): 56.9 μm, under 410x of magnifying.



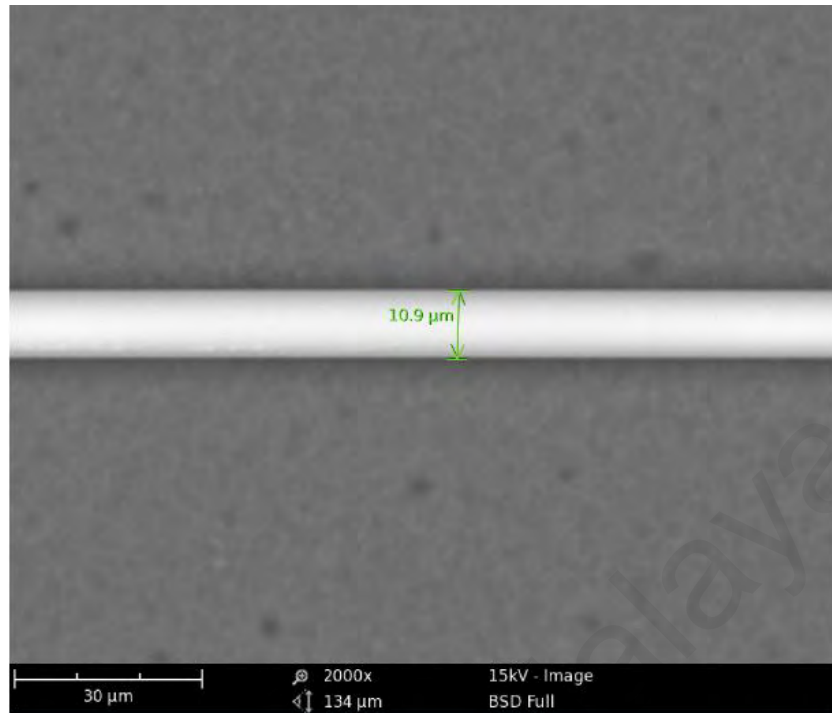
(d): Etched (15 mins): 28.2 μm, under 1000x of magnifying.



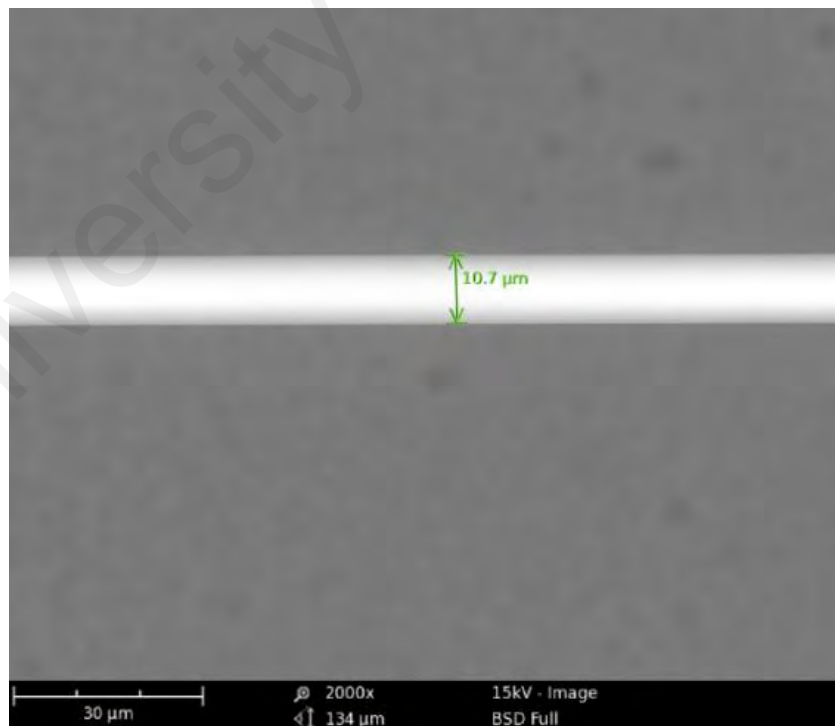
(e): Etched (18 mins): 12.5 μm, under 2000x of magnifying.



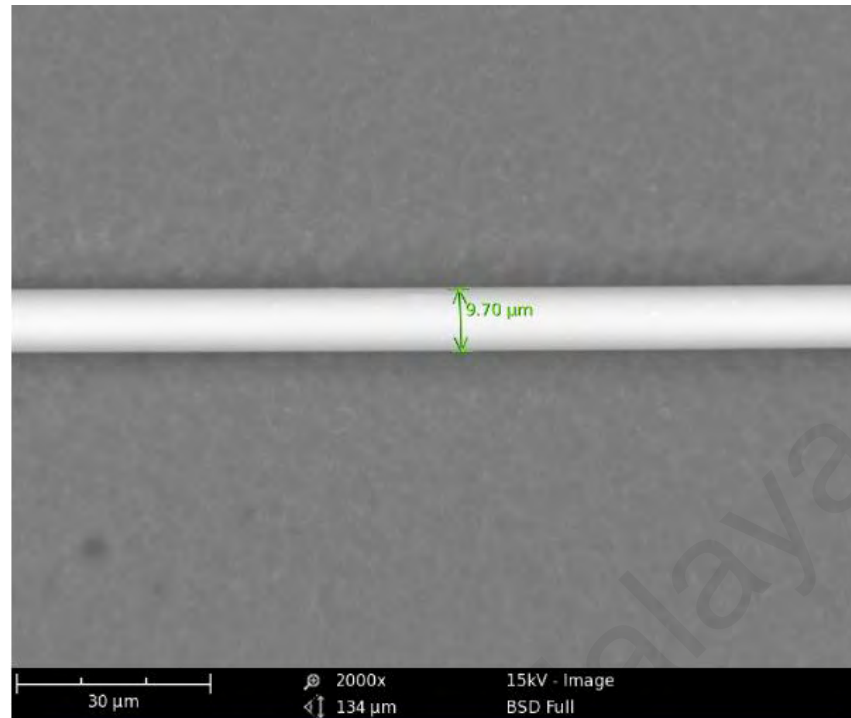
(f): Etched (18 mins): 11.2 μm, under 2000x of magnifying.



(g): Etched (18 mins): 10.9 μm , under 2000x of magnifying.



(h): Etched (18 mins): 10.7 μm , under 2000x of magnifying.



(i): Etched (18 mins): 9.7 μm, under 2000x of magnifying.

Figure 4.5: SEM measurements on, (a) un-etched FBG, (b) 90μm etched, (c) 56.9μm etched, (d) 28.2μm etched, (e) 12.5μm etched, (f) 11.2μm etched, (g) 10.9μm etched, (h) 10.7μm etched, (i) 9.7μm etched.

4.2.1 Sensitivity Characterization of Etched Fibers

The dependence of sensitivity of sensors on ethanol concentration in terms of wavelength shift has been analyzed to study the FBG sensitivity with its cladding diameters. The results of ethanol concentration measurements via different FBG cladding diameters are shown in Figure 4.6.

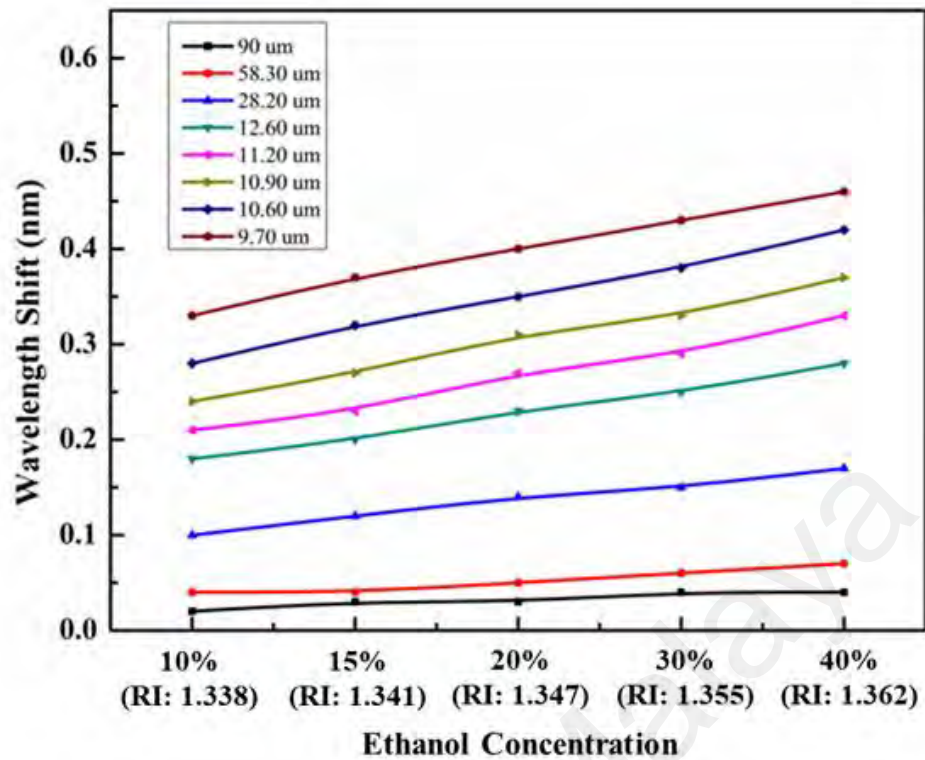


Figure 4.6: Bragg wavelength shift for different FBG thickness under different ethanol concentration.

It is observed that the peak wavelength has shifted 0.46 nm for FBG with 9.7 μm diameter in an ethanol concentration of 40%; as compared to a 10% ethanol concentration with a 0.33 nm peak wavelength shifts. This is due to the higher RI of 1.362 in 40% concentration as compared to RI 1.338 in 10% of concentration. The RI of ethanol changes the effective index of the FBG and Bragg wavelength shifts to longer wavelength in higher concentration ethanol with higher RI, as stated in equation 2.8.

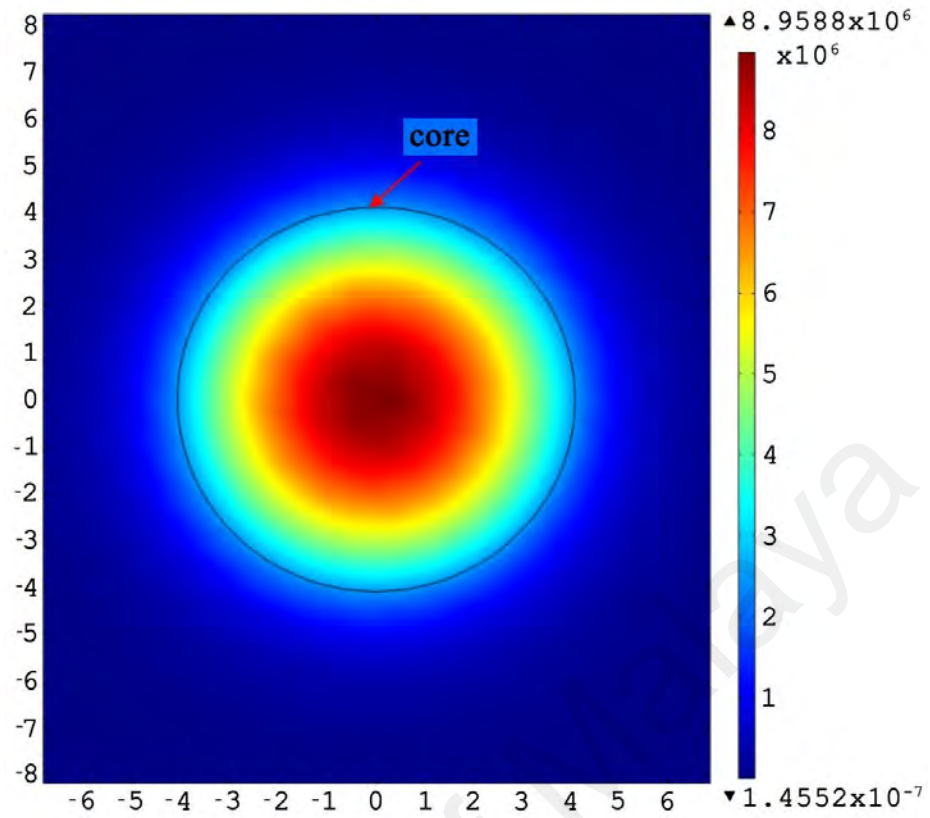
Hence, this can conclude that the FBG wavelength shifted more with a thinner diameter as close as to the core diameter, regardless of any concentrations of ethanol. This proved that the FBG is more sensitive when the cladding diameter is reduce. The evanescent field interaction with the surrounding environment will be increased, and this significant changes in the effective RI occur due to surrounding medium RI which leads to Bragg wavelength shifts.

However, based on the numerical analysis shows that, the effective RI of the fundamental core mode was not sensitive to the surrounding RI for cladding diameter greater than 20 μm . (Agostino Iadicicco, Andrea Cusano & Stefania Campopiano, 2005) (Bin-bin Luo, Xiao-jun Zhou, Ming-fu Zhao,b, Nian-bing Zhong & Sao-fei Wang, 2010). Thus the results on the wavelength shift for FBG diameter greater than 20 μm are suspected due to the effects of surrounding temperature.

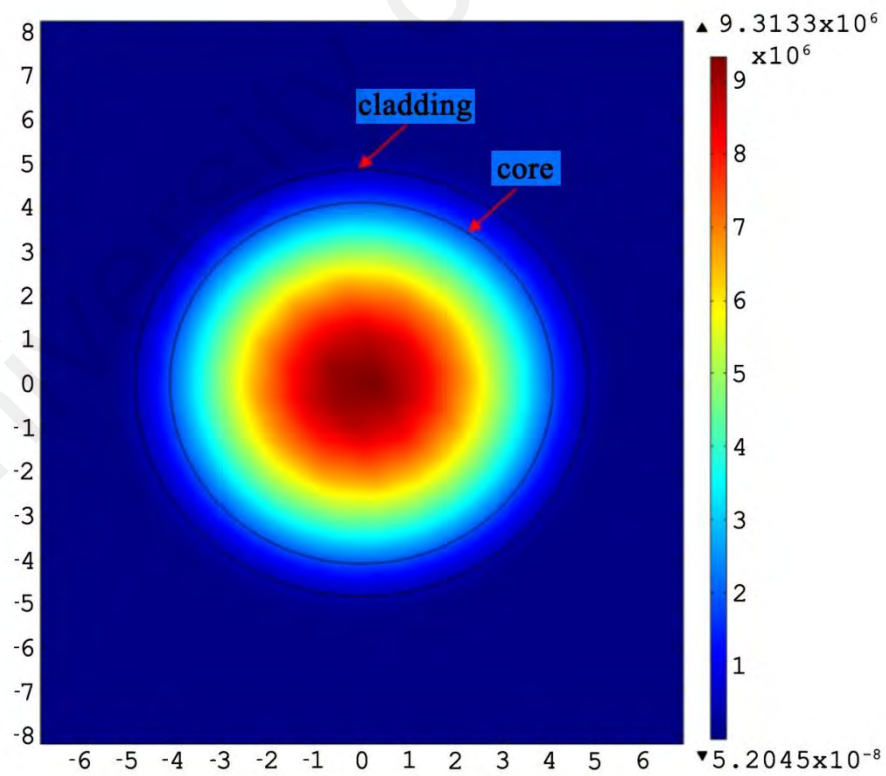
Therefore, with these results, 9.7 μm FBG diameters is chosen for the development of corrosion sensors. The results were further supported by COMSOL simulation result that will be discussed in the following section.

4.3 Study of Evanescent Field in Etched Fiber

Evanescent field in the fiber optic is modeled to study the effects of etching to the fiber sensor sensitivity. The field distribution was modeled using COMSOL Multiphysics 5.0 simulation software for different fiber cladding diameter. Figure 4.7 (a) and 4.7 (b) show the field distribution in fiber with 125 μm diameters (unetched) and after etched to the core as 9.7 μm , respectively.



(a): Un-etched: 125 μm fiber diameter.



(b): Etched - 9.7 μm fiber diameter.

Figure 4.7: COMSOL simulation on etched and un-etched fiber.

Figure 4.8 below shows the fiber diameter power distribution calculated by COMSOL via the below equation (Arif, Ahmed, Asaduzzaman, & Azad, 2016):

$$f = \frac{\int_{\text{sample}} (E_x H_y - E_y H_x) dx dy}{\int_{\text{total}} (E_x H_y - E_y H_x) dx dy} \quad (4.1)$$

Where, f is the fiber power distribution in fiber core; E_x , E_y and H_x , H_y are the transverse electric fields and magnetic fields of the mode, respectively. The higher of the f value, the better sensitivity of the fiber. The mode field pattern E_x , E_y and H_x , H_y can be simulated with the COMSOL simulation software.

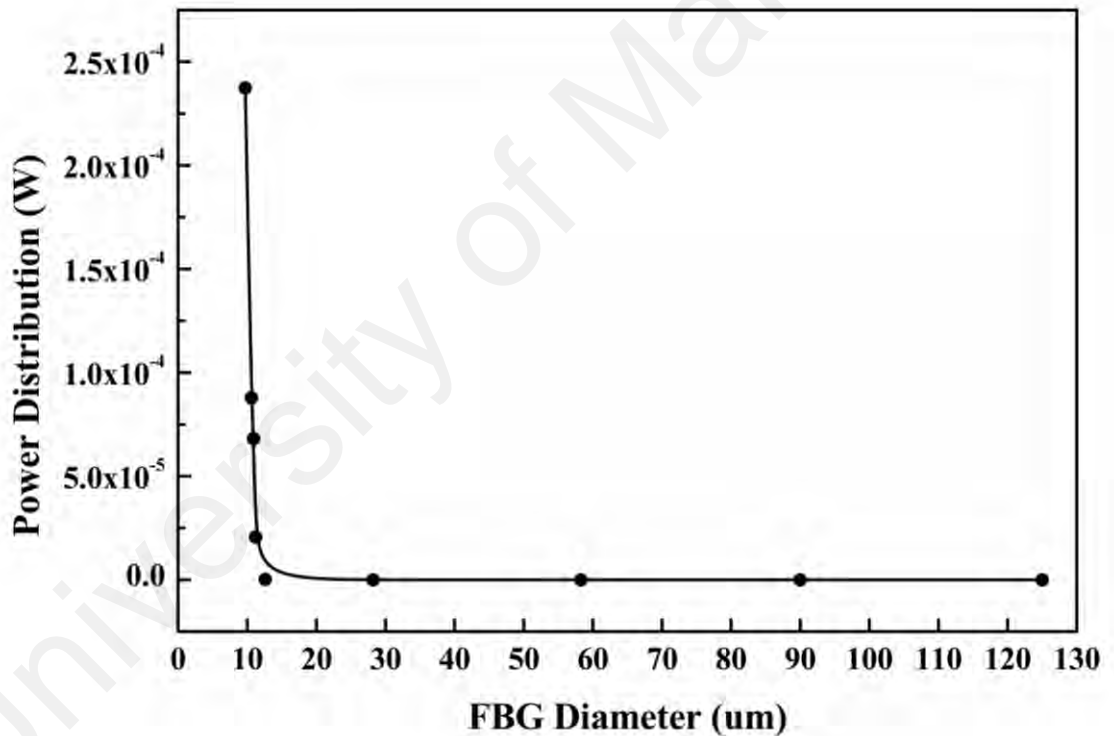


Figure 4.8: Power distribution for different FBG diameter.

It is observed that the power distribution is exponential decay to the fiber diameter. Thinner FBG diameter corresponds to a higher power distribution. The COMSOL simulation result has reported power distribution of 4.06×10^{-21} W for a 90 μm diameter. A higher power distribution of 2.37×10^{-4} W is being observed when the diameter is reduced to 9.7 μm . It is visible that with the decrease of FBG diameter leads to

penetrate more evanescent field through the cladding which leads to enhance the sensitivity significantly. These were also proved with the ethanol concentration sensitivity experiment as per section 4.2.1.

4.4 PDMS Coating Characterization

In order to effectively measure for early corrosion detection, it is necessary to modify the package structure of FBG sensors. This was achieved by packaging these sensors in a high-molecular compound known as the Polydimethylsiloxane (PDMS).

FBG was coated with PDMS of 0.5mm thickness in an aluminum plate and the rebar was carefully placed on it. Non-coated FBG was placed beside the coated FBG as references. The rebar was exposed to the 80% of humid environment, measured by humidity meter (Extech, SDL 550), to induce and accelerate the corrosion process. The FBG wavelength shifts for both coated and non-coated samples were monitored daily via FBGA, recorded and examined until the rebar is corroded. Figure 4.9 shows the corroded rebar on day-70. The observation and measurements were carried on until the FBG wavelength shift become constant for 100 days.

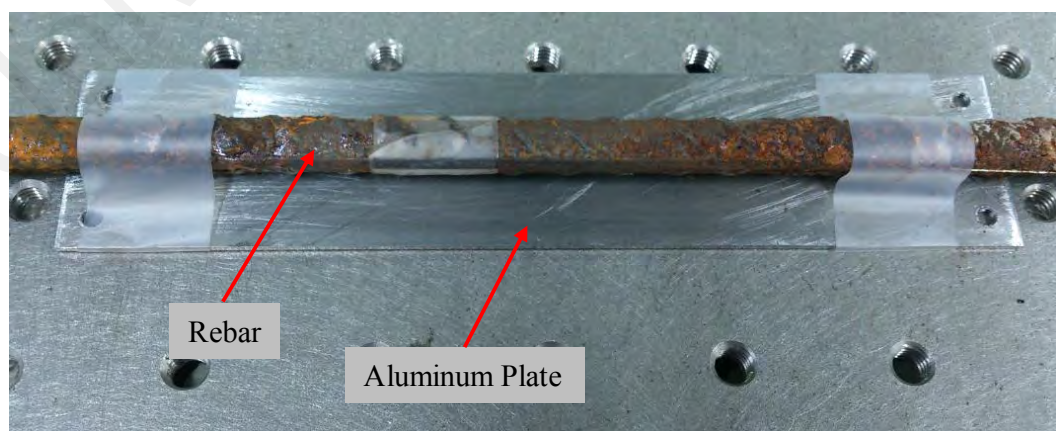


Figure 4.9: Corroded Rebar.

4.4.1 Corrosion Rate

The corrosion rate is usually expressed as the mass loss or thickness loss of a metal with time. It also can be measured as a rate of weight loss. The corrosion rate is important to justify the risk of a building structure by knowing its corrosive category via mass loss (Landolfo, Cascini, & Portioli, 2010). The corrosive categories were justified under the specifications of BS EN 12500:2000 (“ASTM G102 : Standard Practice for Calculation of Corrosion Rates and Related Information from Electrochemical Measurements,” n.d.), a worldwide standard for structural monitoring in civil engineering, as per Table 4.1 below.

Table 4.1: Corrosiveness Category under BS EN 12500:2000 for four common materials.

Steel (mm/year)	Zinc (mm/year)	Copper (mm/year)	Aluminum (mm/year)	Corrosiveness category	
≤10	≤0.7	≤ 0.9	Negligible	Very low	C1
10–200	0.7–5	0.9–5	≤0.6	Low	C2
200–400	5–15	5–12	0.6–2	Medium	C3
400–650	15–30	12–25	2–5	High	C4
650–1,500	30–60	25–50	5–10	Very high	C5

The corrosion rate is the speed at which any given metal deteriorates in a specific environment, and any different units are able to use to express the corrosion rate. Using the unit as stated in equation 2.6 for W, A, T and D, the corrosion rate can be calculated in a variety of units with the appropriate value of K. In this experiment, $K = 8.76 \times 10^4$ (constant value for rebar per BS EN 12500:2000 standard) is used to calculate the corrosion rate and the corrosion unit is in mm/year.

4.4.2 Results and Discussion

The performance of etched FBG (9.7 μ m diameter) with PDMS coatings and non-coated sample, are shown in Figure 4.10. It is also observed the FBG wavelength shifts are in a proportional linear relationship with corrosion rate through the corrosion process, as shown in Figure 4.11.

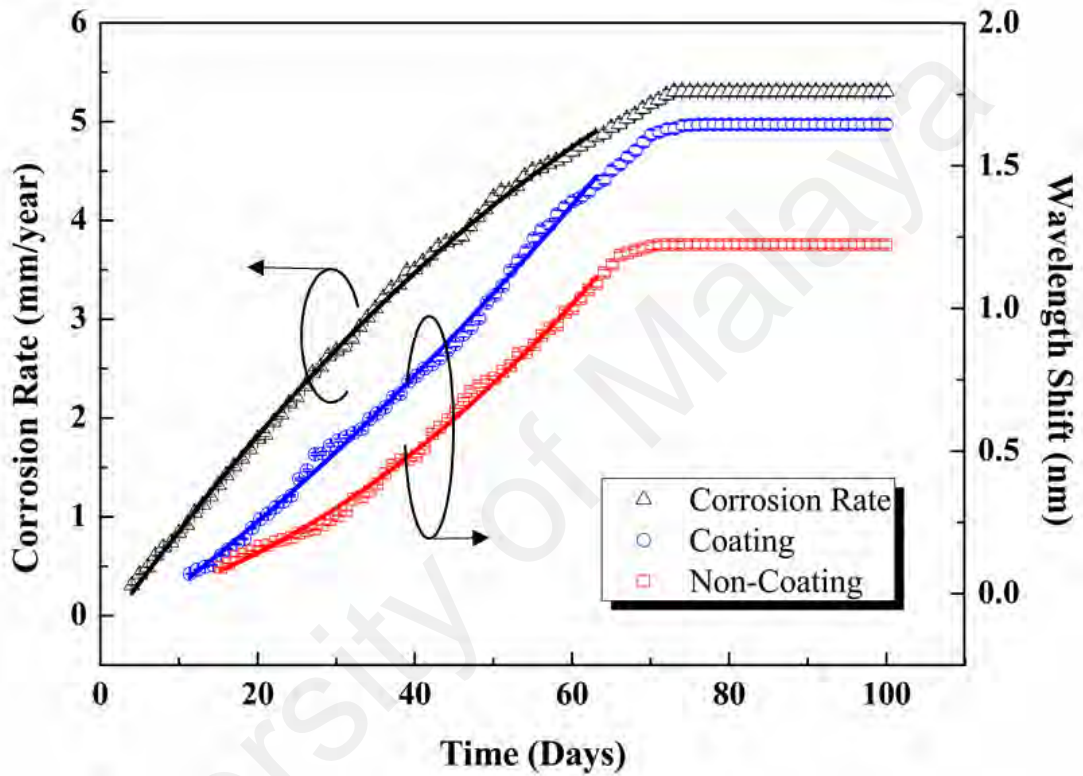


Figure 4.10: Wavelength shift and corrosion rate by days.

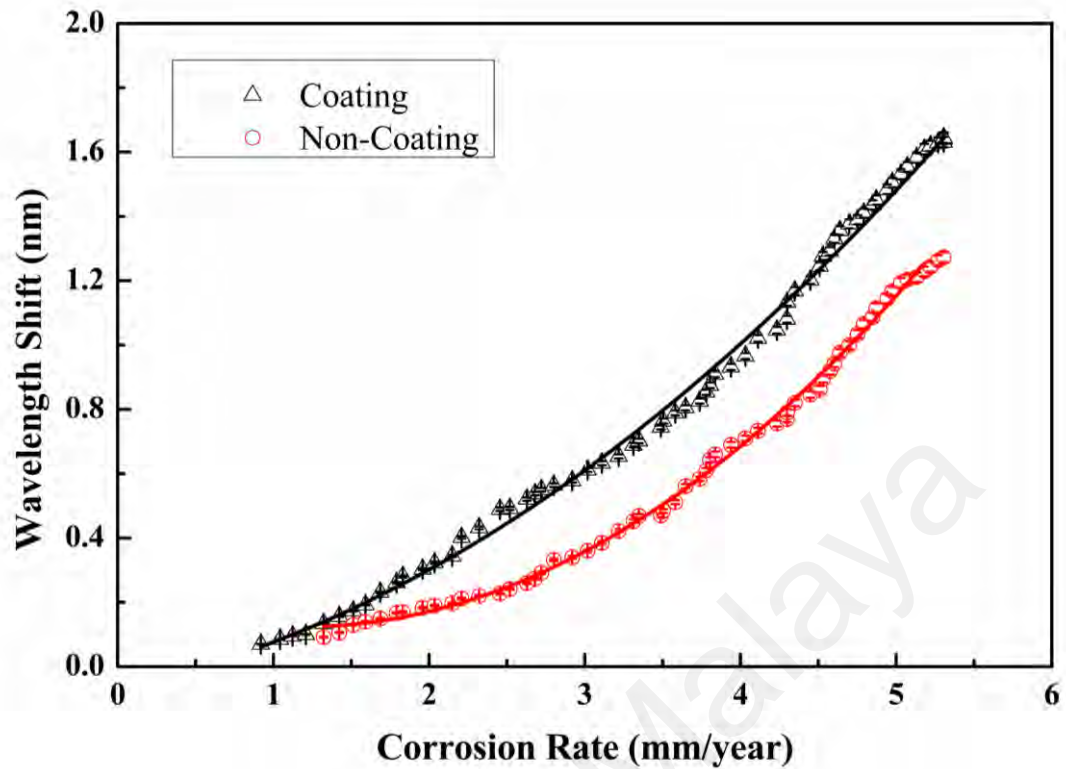


Figure 4.11: Wavelength shift by corrosion rate.

From this experiment work, it is observed that the wavelength shift shows an earlier detection after day-10 for FBG coated PDMS as compared to the FBG without PDMS coating at day-16.

In addition, we need to immediately stop the cleaning process once the corrosion surface has been cleaned. Repeated cleaning on the sample by HCL acid would easily etch out the sample and causing inaccurate results.

It is observed the rebar started to corrode on day-18 with a rust layer started to form on the surface, and the corroded rust layer continues to form and induces greater strain effect causing a wavelength shift up to day-77.

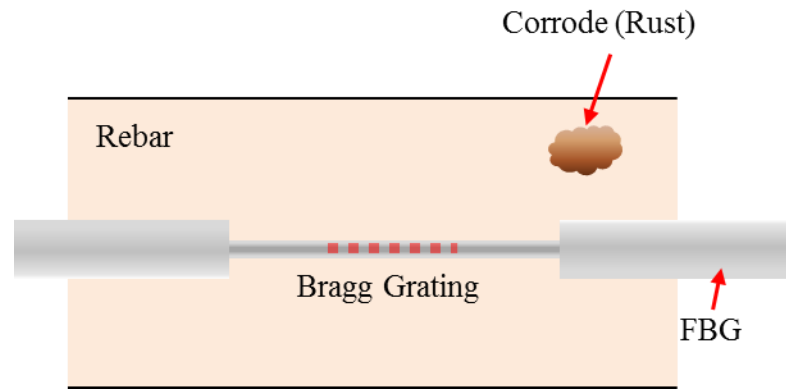
On day-77, the FBG wavelength with PDMS coating significantly shifted 1.65 nm. As for the FBG wavelength without coating, it shifted only 1.21 nm, which was 0.44 nm less as compared to the FBG with PDMS coating. On the other hand, the corrosion

rate was calculated via conventional weight loss method as a reference rebar to the FBG wavelength shift. Observed the corrosion rate is increasing proportionally with the wavelength shift. However, the corrosion rate becomes constant at day-73, which was 4 days earlier as compared to FBG wavelength shift at day-77.

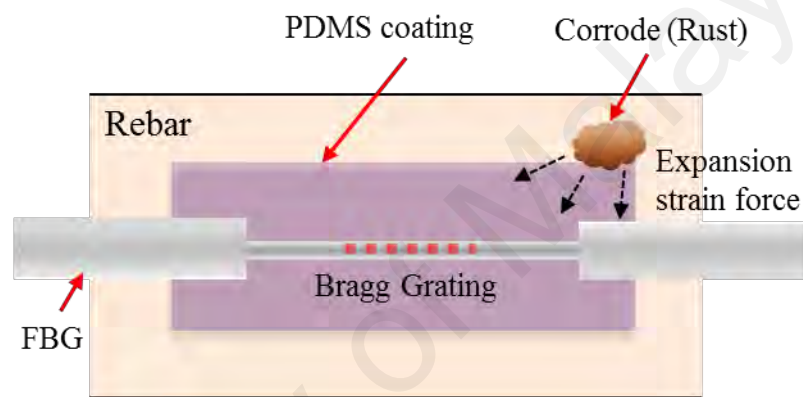
This could be due to the corrosion process and the rust formation started to slow down after 70 days, where it might not be sensitive and accurate to measure via conventional method. The small rust formation could be easily detected by FBG sensor.

In general, the 9.6 μm etched FBG sample with PDMS coating performed better in sensing and showed earlier detection after 10 days at a sensitivity of 1.65 nm/ mm/ year as compared to the FBG without coated at 1.21 nm/ mm/ year.

PDMS coated FBG sensors shows an earlier detection can be further explained by the mechanical properties of PDMS, which is a soft mixture with elastic features (Kersey et al., 1997), conformable and compliant material. With PDMS coating, it becomes a media to transfer the corrosion-induced strain to the Bragg grating (Wang, 2011). When the corrosion gets into contact with the PDMS layer, the strain will be transferred and extend the force to the Bragg grating, causing the wavelength shift. Whereas, for the FBG without coating, the corrosion rust needs to be closely contacted with the Bragg grating to induce the wavelength shift, as shown in Figure 4.12 below. Therefore, with PDMS coated FBG sensor, it is able to enhance the sensing capability of FBG for early corrosion detection.



(a): Mechanism without PDMS coating.



(b): PDMS mechanism act as strain transfer media.

Figure 4.12: PDMS mechanism.

Nevertheless, from the experimental work, corroded rebar induced strain was monitored by the FBG through the observation on their reflected wavelengths. Once the FBG is bonded onto or embedded into the test structure, the expansion of the structure material causes a change in the grating period. The strain, ε_m induced in the Bragg wavelength shift can be derived through the measuring of wavelength shift, λ_B according to the relation, given by (Liu et al., 2003):

$$\frac{\Delta\lambda_B}{\lambda_B} = (1 - p_e)\varepsilon \quad (4.2)$$

Where, p_e is the optical fiber elasto-optic coefficient with the value of 0.22 for germanosilicate fiber, and $1 - p_e$ often know as constant, $k = 0.78$.

The temperature sensitivity of the Bragg wavelength arises from the change in the period associated with the thermal expansion of the fiber (Minh Châu Phan Huy, 2010, Martin J. O'Dwyer, 2004). Temperatures changes affect both the effective index and grating period of an FBG. FBG is also sensitive to external strain and thus requires temperature compensation when a corrosion sensing has to be performed.

Since it has been proven that the temperature as one of the factors that could affect the wavelength shift, thus below equation is used for temperature compensation for strain calculation:

$$\epsilon_m = \frac{1}{k} * \frac{\Delta\lambda_B}{\lambda_B} - \left(\alpha_{sp} + \frac{\alpha_s}{k} \right) * \Delta T \quad (4.3)$$

Where;

α_{sp} = Thermal expansion coefficient of the material = $3.10 \times 10^{-4} \text{C}^{-1}$

α_s = Thermo-optic coefficient of the material = $8.6 \times 10^{-6} \text{C}^{-1}$

$\Delta T = T_1 - T_0$

The relationship of strain-induced and corrosion rate by days are shown in Figure 4.13 below with R^2 equal to 99.73% for corrosion rate and 99.89% for the induced-strain, whereas Figure 4.14 shows the linear relationship between induced-strain and corrosion rate ($R^2 = 99.86\%$). Strain was calculated by using the equation 4.3 with temperature compensation as a noise factor throughout the experiment. Therefore, the strain value should represent the actual strain induced by rebar corrosion (“Strain Measurement with Fiber Bragg Grating Sensors | HBM,” n.d.). As R^2 is close to 100%,

it can be concluded that there is a proportional relationship between the corrosion rate and induced-strains.

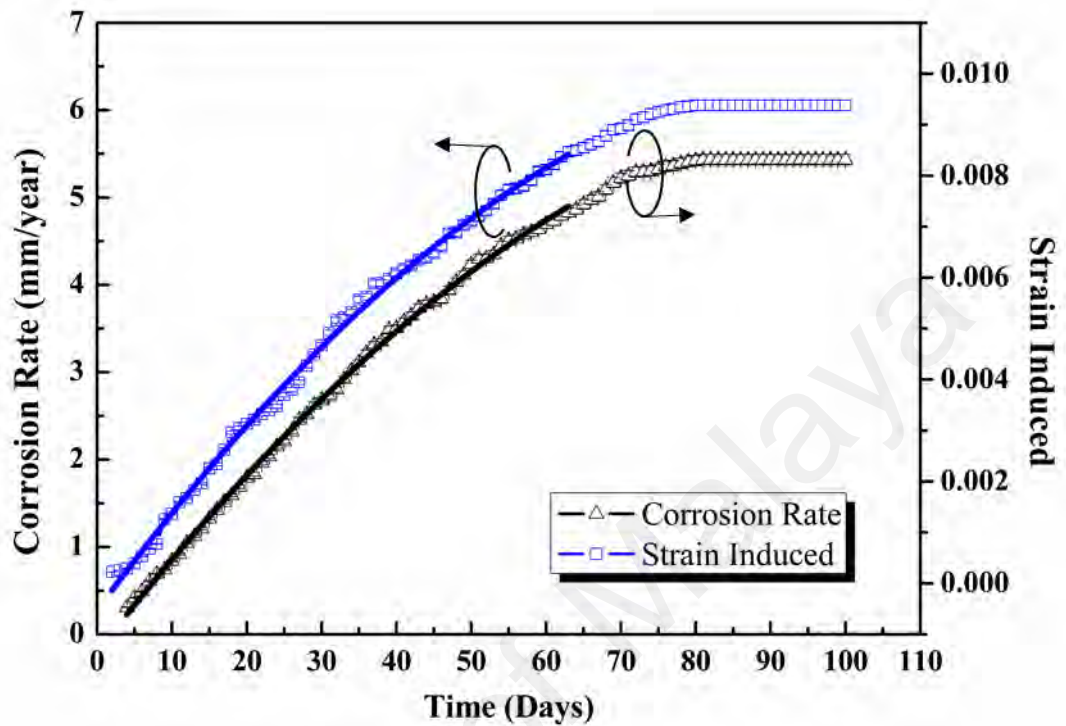


Figure 4.13: Relationship between corrosion rate and strain induced by time.

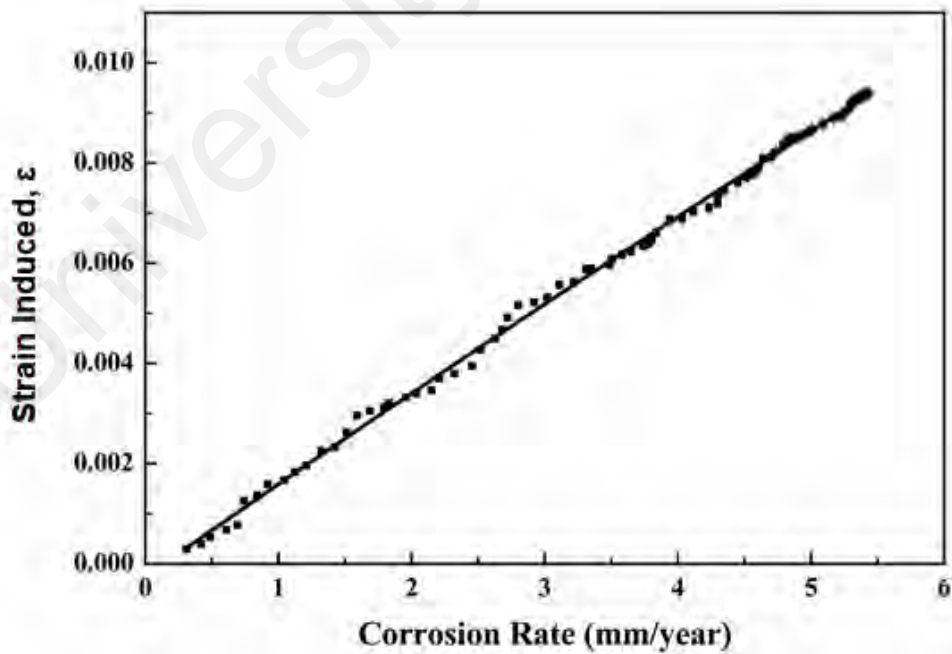


Figure 4.14: Strain induced vs corrosion rate.

4.5 Hydrogel-Coated FBG Characterization

Etched FBG coated with hydrogel-PDMS mixture were developed and monitored. The FBG sensors were embedded on the rebar for corrosion monitoring over 100 days until the rebar get corroded. This work was focused on exposed rebar structures with hot and humid weather of Asia. Hydrogels are made up of cross-linked polymers chain and an aqueous solution, which absorb water and swell to an appreciable extent in water (Majumder et al., 2008) (Ahmed, 2015). The swelling and shrinking action of the hydrogels are readily converted to a mechanical response in the form of force and is the basis of the detection process in the present sensor.

Therefore, with the present of the hydrogel as a coating layer, the mechanical expansion will stretch the FBG and the fiber grating would expand, which caused the changing in grating period, thus increases the Bragg wavelength shift.

In order to enhance the sensitivity of strain induced by corrosion, a mixed solution of PDMS and hydrogel were developed as a coating layer on FBG sensor. Different ratio mixtures were tried out and a ratio of 0.15 hydrogel: 0.85 of PDMS were finalized to be coated on FBG. This ratio shows its stability in forming a solid layer.

Both PDMS and hydrogel solutions were prepared in the designated ratio and stirred for 5 mins to mix well. The mixture solution was then placed at room temperature for 20 minutes to remove trapped bubbles. The rebar was mounted on aluminum together with fiber and the mixture solution, as shown in Figure 3.6 above.

Figure 4.15 below shows the structure of PDMS mixed Hydrogel coated in etched FBG sensor FBG Bragg wavelength shift along the corrosion process was monitored and recorded via FBGA.

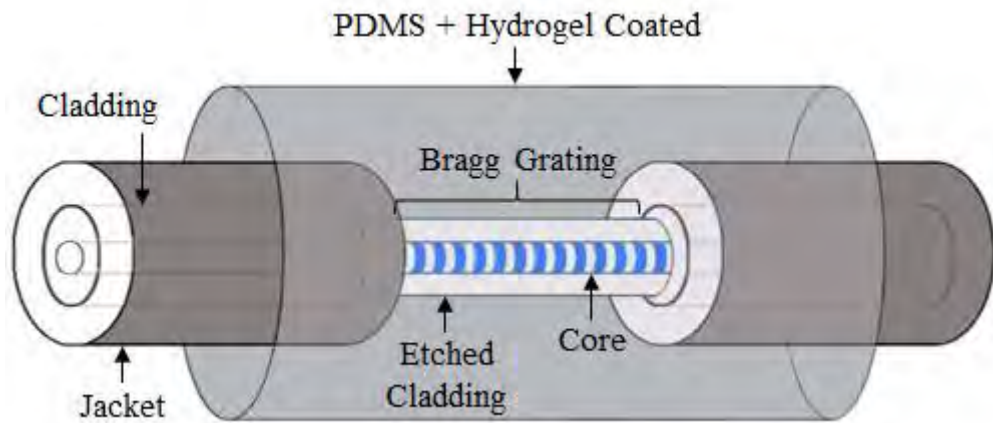


Figure 4.15: Structure of PDMS-Hydrogel coated in etched FBG.

Figure 4.16 below shows the FBG peak wavelength after coated at wavelength of 1547.38 nm. It is observed that, the wavelength shifted 0.14 nm from 1547.24 nm. This can be explained by the stretch effect due to the cross-linking of PDMS formation from liquids to solid state (Shuhui Liu et.al, 2019) (L. Dorogin & B.N.J. Persson, 2018).

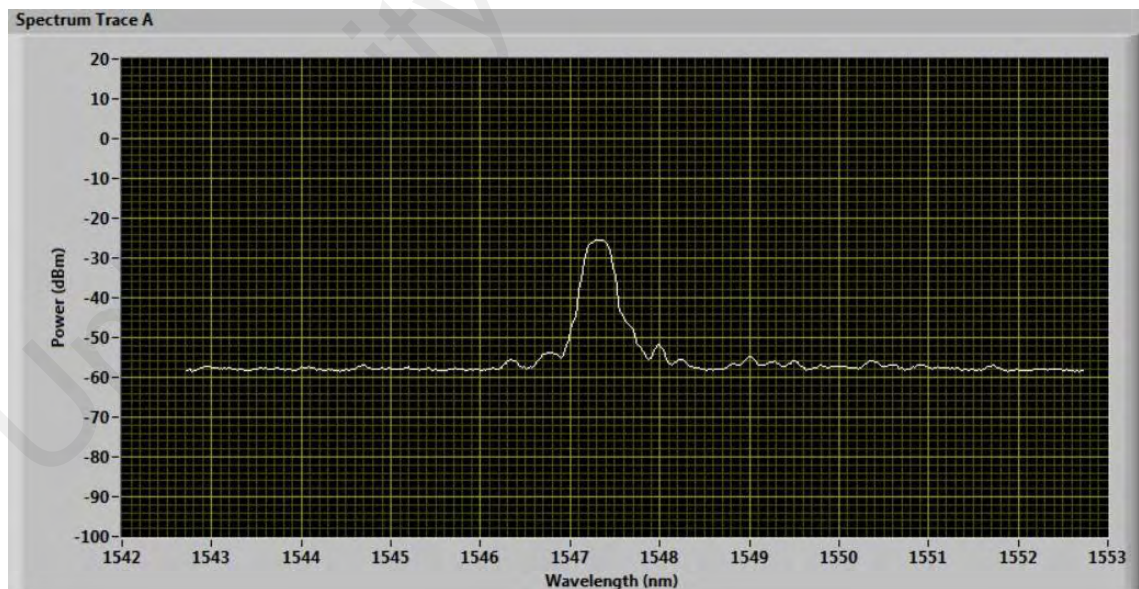


Figure 4.16: FBG wavelength before and after coating at 1547.38 nm.

4.5.1 Results and Discussion

Figure 4.17 depicts the wavelength shift through the corrosion process in a comparison between PDMS and PDMS-hydrogel coated FBG which shows the linear relationship between PDMS FBG ($R^2 = 99.77\%$) and PDMS-hydrogel ($R^2 = 99.89\%$). It is observed that the FBG wavelength started to shift on day-8 for PDMS-hydrogel FBG sensor compared to day-11 for PDMS FBG sensor. A significant higher wavelength shift observed occurred on PDMS-hydrogel FBG sensor on day-61 onwards compared to PDMS FBG sensor. This could be explained that H^+ ions formation accumulated through the corrosion process from day-1. Thus, with more H^+ ions, it tends to react with hydrogel and causing the wavelength shift higher as compared to only PDMS FBG.

In addition, it is observed that the wavelength shift for PDMS-hydrogel becomes constant on day-83 onwards, which was 6 days later compared to PDMS FBG sensor. This could be due to the corrosion process are still producing H^+ ions, and these H^+ ions are not able to be detected by the PDMS FBG sensor which is strain sensitive material.

Generally, PDMS-hydrogel FBG sensor demonstrates better performance in corrosion detection with sensitivity of 1.97 nm/ mm/ year compared to the PDMS FBG sensor with sensitivity of 1.65 nm/mm/year.

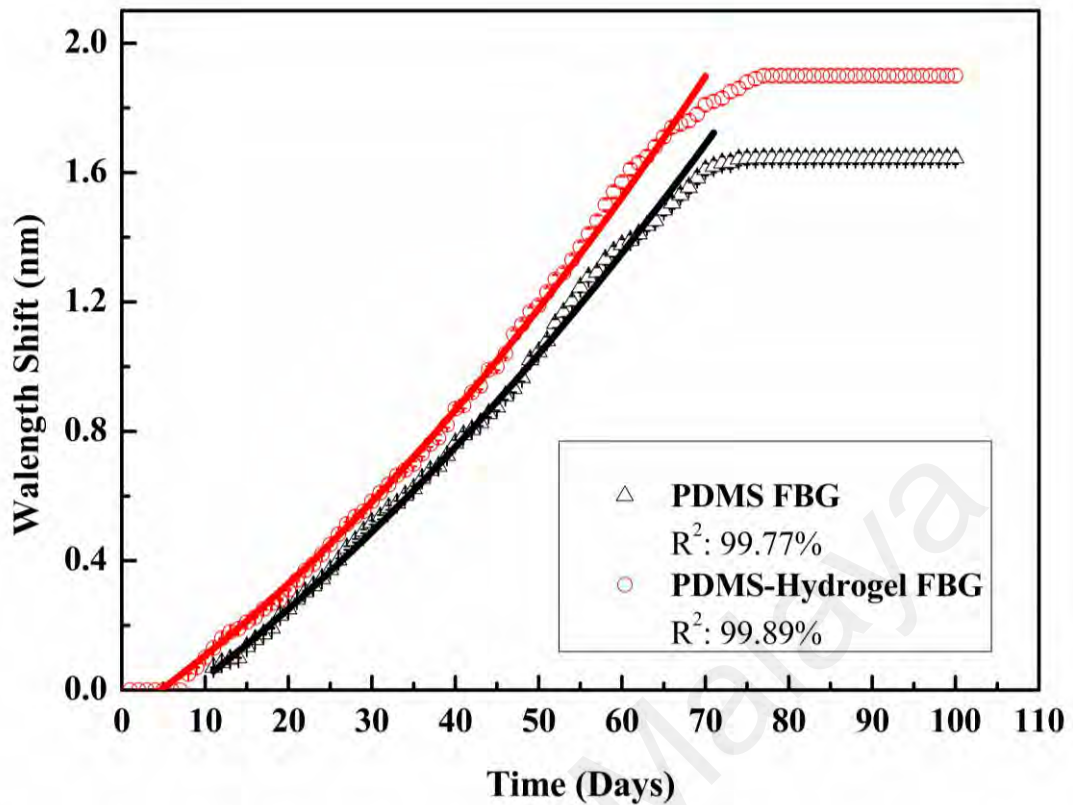


Figure 4.17: FBG wavelength shifts comparison PDMS and PDMS-Hydrogel sensor.

Corrosion rate was measured via mass loss method for comparison with PDMS-hydrogel and PDMS FBG sensor, as illustrated in Figure 4.18.

It is observed that there is a positive relationship between the wavelength shift and the corrosion rate for PDMS FBG and PDMS-hydrogel FBG, with R^2 equal to 99.69% and 99.83%, respectively. Overall, the corrosive category in this research work is under C1 per ASTM standard specification BS EB 12500:2000 (“ASTM G102 : Standard Practice for Calculation of Corrosion Rates and Related Information from Electrochemical Measurements,” n.d.), as stated in Table 4.1 above.

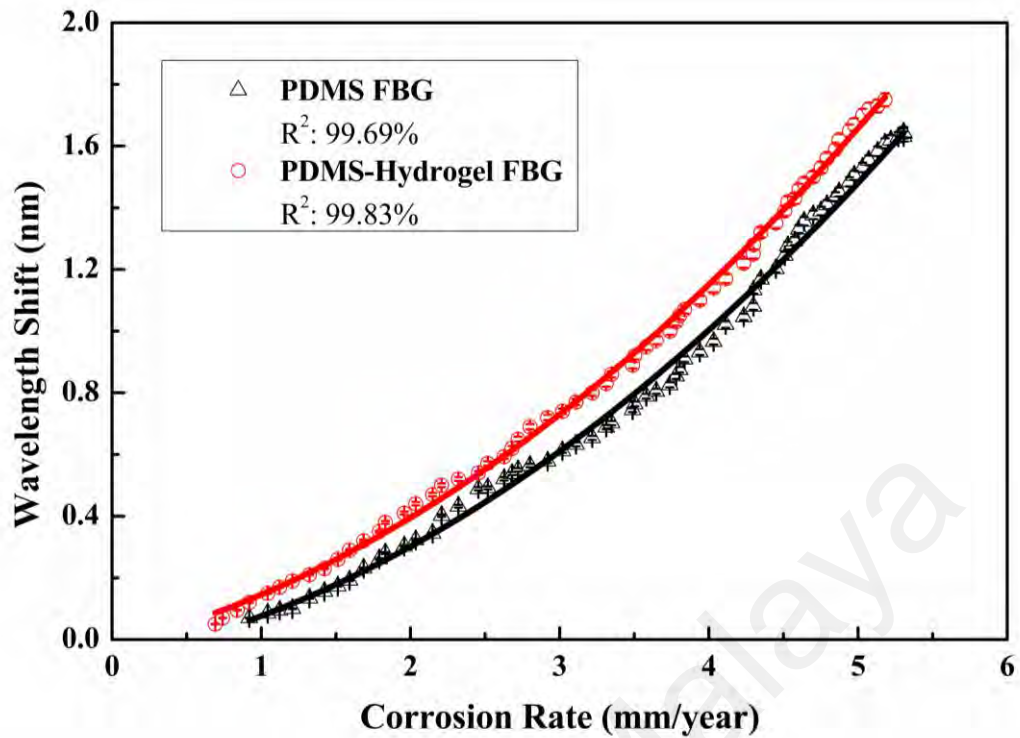


Figure 4.18: FBG wavelength shift by corrosion rate for PDMS and PDMS-Hydrogel sensor.

Due to the swelling properties of the hydrogel, tensile stress and a mechanical expansion were applied on the FBG, resulting in more significant FBG wavelength shift. Besides the swelling effect from the hydrogel, the small amount of PDMS itself acts as the contact layer to transferred and extends the stress to the Bragg grating and hence causing the wavelength shift. Both mixture solutions could interact with each other to produce a better sensitivity sensor for early corrosion detection.

In general, PDMS-hydrogel FBG sensor shift demonstrated much higher sensitivity with 1.98 nm/ mm/ year, compared to PDMS FBG sensor with 1.65 nm/ mm/ year.

4.6 Chapter Summary

Fiber sensors for corrosion monitoring in SHM were developed and characterized. FBG sensors with and without PDMS coatings were studied for early corrosion detection which can be applied in the near future, especially in civil engineering for SHM systems. The overall result shows that, there is a linear relationship between the wavelength shifts along the corrosion process due to the corrosion strain force. The cladding-etched FBG (9.7 μm diameter) with PDMS coatings demonstrated much higher sensitivity for corrosion detection compared to un-etched FBG. This is because PDMS helps to act as a media to expand the corrosion strain force to the FBG.

In addition, PDMS-Hydrogel coated etched FBG was also characterized, studied and compared for the performance on corrosion detection sensitivity. PDMS-hydrogel demonstrated better sensitivity in corrosion detection, which could be due to the presence of the H^+ ions that generate during the corrosion process. Since the hydrogel are sensitive to the pH and the properties of swelling effect from hydrogel when interact with acidic pH, thus the expansion from the coating with help from PDMS are able to increase the FBG sensitivity.

Overall, results show there is a proportional relationship between Bragg wavelength shift along the corrosion process with the strain force induced. PDMS-hydrogel FBG sensor shift demonstrated much higher sensitivity with 1.98 nm/ mm/ year, compared to PDMS FBG sensor with 1.65 nm/ mm/ year. Therefore, with the results from this research work, this proves that it is feasible to develop FBG based sensing system as non-destructive real-time corrosion detection for SHM system.

CHAPTER 5: CONCLUSION AND FUTURE RECOMMENDATION

5.1 Conclusion

This thesis presents in-depth studies on early corrosion detection via two different FBG coating for SHM system based on fiber Bragg gratings sensors.

First, the study of sensitivity of FBG via wet etching was carried out and discussed. In this study, the cladding of FBG was wet etched by HF acid. It is observed that 9.7 μm etched FBG demonstrated higher sensitivity. On the other hand, COMSOL modeling was carried out to simulate and calculate the intensity of each FBG diameters, to further support the FBG sensitivity. This verified that by reducing the FBG thickness; the higher sensitive of the FBG.

FBG sensors with and without PDMS coatings were studied for early corrosion detection. The overall results of the two different fiber diameters show that, there is a linear relationship between the wavelength shifts along the corrosion process due to the corrosion-induced strain. In addition, the cladding-etched 9.7 μm FBG with PDMS coatings demonstrated much higher sensitivity for corrosion detection. It was observed that, wavelength shifted 1.65 nm on day-77 for PDMS coated sensor, compared to 1.21 nm for non-coated sensor. This is due to the fact that PDMS helps to act as a media to expand the corrosion strain force to the FBG sensor. It is also observed the wavelength remain constant after day-77. Therefore, from this research, this approach with the FBG based sensing system is able to provide a real time early corrosion detection system for long term SHM applications, with the sensitivity of 1.65 nm/ mm/ year for PDMS-FBG, compared to non-coated FBG at 1.21 nm/ mm/ year.

To further enhance the sensitivity for early corrosion detection, hydrogel-PDMS coated etched FBG sensor has been further developed to suite the corrosion characteristic, where the rust are acidic properties. In this work, PDMS-hydrogel FBG sensor were fabricated and the performances were examined. Not only the strain induced by corrosion caused the wavelength shifted, but the expansion and swelling effect from the coating due to a pH change induced strain and caused the FBG wavelength shifted. This provides earlier corrosion sensing detection as when corrosion induces, the process generates hydrogen ions, H⁺ that caused hydrogel swell and thus, increase the sensitivity. Observed the wavelength shifted 1.97 nm on day 77 for PDMS-hydrogel sensors compared to 1.65 nm for PDMS sensors in the same condition.

Overall, results showing that PDMS-hydrogel demonstrates better performance results, with the sensitivity of 1.97 nm/ mm/ year compared with PDMS coated FBG which sensitivity of 1.65 nm/ mm/ year. With the results from this experiment, this proves that it is feasible to manufacture a pH sensors based FBG as a SHM real time monitoring system.

Table 5.1: The comparison of fabricated FBG sensors in this thesis work with the literature.

Author	Coating / Technique	Sensor System	Sensitivity
Lopez et al., 2017	Polyaniline (PAni) coated FBG	Un-etched pH sensor	0.5 nm / mm / year
Fodan et al., 2016	Hypodermic protective tube coated FBG	Un-etched FBG for corrosion detection	0.05 nm / mm / year
Thesis Work	Un-coated	Etched strain sensor	1.21 nm / mm / year
	PDMS coated FBG	Etched strain sensor	1.65 nm / mm / year
	PDMS-Hydrogel coated FBG	Etched pH sensor	1.97 nm / mm / year

5.2 Future Works

In this research work, FBG for early corrosion system are studied and developed. The works presented are mainly on the development of FBG sensitive coating for corrosion detection by using PDMS and hydrogel material. Nevertheless, there are still some works that still need to be addressed in the future. This research works focus on the lab experiment to developed a novel fiber sensor for early corrosion detection. Therefore, it is suggested that the appropriate protective coating for the FBG should be studied and developed in future for the installation on marine building structure, which the rebar is exposed to the sea. Handling of the fibers during installation to the structural building is also equally important since FBG is fragile and sensitive to strain and temperature. In addition, environmental factor such as temperature that could influence Bragg wavelength shift must be accounted for to implement a practical FBG-based SHM system. Generally, this technique can be implemented to other area for corrosion monitoring as well, such as pipelines and tanks monitoring, especially on oil and gas industry.

REFERENCES

- 4 Societal Benefits of Structural Health Monitoring (SHM). (n.d.). Retrieved September 3, 2019, from <https://graduatedegrees.online.njit.edu/blog/4-societal-benefits-of-structural-health-monitoring-shm/>
- Agostino Iadicicco, Andrea Cusano & Stefania Campopiano (2005). Thinned Fiber Bragg Gratings as Refractive Index Sensors. *IEEE Sensors Journal*, Vol. 5 (6). <https://doi.org/10.1109/JSEN.2005.859288>.
- Agrawal, A. K. (2001). Corrosion Monitoring. In *Encyclopedia of Materials: Science and Technology* (pp. 1698–1701). <https://doi.org/10.1016/B0-08-043152-6/00302-8>
- Agrawal, G. (2013). Introduction. In *Nonlinear Fiber Optics* (pp. 1–25). <https://doi.org/10.1016/B978-0-12-397023-7.00001-2>
- Ahmed, E. M. (2015). Hydrogel: Preparation, characterization, and applications: A review. *Journal of Advanced Research*, Vol. 6, pp. 105–121. <https://doi.org/10.1016/j.jare.2013.07.006>
- AIE | Introduction to Corrosion Coupons. (n.d.). Retrieved September 2, 2019, from <https://www.assetintegrityengineering.com/introduction-corrosion-coupons/>
- Al-Sulaimani, G. J., Kaleemullah, M., Basunbul, I. A., & Rasheeduzzafar. (1990). Influence of corrosion and cracking on bond behavior and strength of reinforced concrete members. *ACI Structural Journal*, 87(2), 220–231. <https://doi.org/10.14359/2732>
- Allard, F. C. (1990). *Fiber optics handbook: for engineers and scientists*. McGraw-Hill.
- Almusallam, A. A., Al-Gahtani, A. S., Aziz, A. R., & Rasheeduzzafar. (1996). Effect of reinforcement corrosion on bond strength. *Construction and Building Materials*, 10(2), 123–129. [https://doi.org/10.1016/0950-0618\(95\)00077-1](https://doi.org/10.1016/0950-0618(95)00077-1)
- Andrade, C., Alonso, C., & Molina, F. J. (1993). Cover cracking as a function of bar corrosion: Part I-Experimental test. *Materials and Structures*, 26(8), 453–464. <https://doi.org/10.1007/BF02472805>
- Antunes, P., Varum, H., & André, P. (2011). Optical FBG sensors for static structural health monitoring. *Procedia Engineering*, 14, 1564–1571. <https://doi.org/10.1016/j.proeng.2011.07.197>
- Arif, M. F. H., Ahmed, K., Asaduzzaman, S., & Azad, M. A. K. (2016). Design and optimization of photonic crystal fiber for liquid sensing applications. *Photonic Sensors*, 6(3), 279–288. <https://doi.org/10.1007/s13320-016-0323-y>
- ASTM. (2008). ASTM G4-01:2008 Standard Guide for Conducting Corrosion Tests in Field Applications. *Annual Book of ASTM Standards*, (Reapproved). <https://doi.org/10.1520/G0001-03>

- ASTM G102: Standard Practice for Calculation of Corrosion Rates and Related Information from Electrochemical Measurements. (n.d.). Retrieved September 3, 2019, from [https://global.ihs.com/doc_detail.cfm?document_name=ASTM G102&item_s_key=00109688](https://global.ihs.com/doc_detail.cfm?document_name=ASTM_G102&item_s_key=00109688)
- Bao, X., & Chen, L. (2012, July). Recent Progress in Distributed Fiber Optic Sensors. *Sensors (Switzerland)*, Vol. 12, pp. 8601–8639. <https://doi.org/10.3390/s120708601>
- Bin-bin Luo, Xiao-jun Zhou, Ming-fu Zhao, Nian-bing Zhong & Sao-fei Wang (2010). Recent developments in microstructured fiber Bragg grating refractive index sensors. *SPIE Reviews*. <https://doi.org/10.1117/6.0000002>.
- Broomfield, J., Rodriguez, J., Ortega, L., & AM, G. (1994). Corrosion rate measurements in reinforced concrete structures by a linear polarization device. *ACI Special Publication, SP 151-9*, 163–181. <https://doi.org/10.14359/4348>
- Chan, T. H. T., Yu, L., Tam, H. Y., Ni, Y. Q., Liu, S. Y., Chung, W. H., & Cheng, L. K. (2006). Fiber Bragg grating sensors for structural health monitoring of Tsing Ma bridge: Background and experimental observation. *Engineering Structures*, 28(5), 648–659. <https://doi.org/10.1016/j.engstruct.2005.09.018>
- C. H. Tan, Shee, Yap, & Adikan, (2016). Fiber Bragg grating based sensing system: Early corrosion detection for structural health monitoring. *Sensors and Actuators, A: Physical*, 246, 123–128. <https://doi.org/10.1016/j.sna.2016.04.028>
- Cheung, P., Toda-Peters, K., & Shen, A. Q. (2012). In situ pressure measurement within deformable rectangular polydimethylsiloxane microfluidic devices. *Biomechanics*, 6(2). <https://doi.org/10.1063/1.4720394>
- Chilingar, G. V, & Mourhatch, R. (2008). Fundamentals of Corrosion and Scaling for Petroleum and Environmental Engineers. In *Fundamentals of corrosion and sacling for petroleum engineers*.
- Christos Markos, Kyriakos Vlachos & George Kakarantzas (2012). Guiding and thermal properties of a hybrid polymer-infused photonic crystal fiber. *Optical Society of America. Optical Materials Express*, 7 (2).
- Cooper, K. R., Elster, J., Jones, M., & Kelly, R. G. (n.d.). Optical fiber-based corrosion sensor systems for health monitoring of aging aircraft. *2001 IEEE Autotestcon Proceedings. IEEE Systems Readiness Technology Conference. (Cat. No.01CH37237)*, 847–856. <https://doi.org/10.1109/AUTEST.2001.949466>
- Culshaw, B., Building, R. C., Street, G., & G, G. (2004). OPTICAL fibre sensors – applications and potential. *7th International COnference on Optoelectronics, Fiber Optics and Photonics*.
- El Maaddawy, T., & Soudki, K. (2007). A model for prediction of time from corrosion initiation to corrosion cracking. *Cement and Concrete Composites*, 29(3), 168–175. <https://doi.org/10.1016/j.cemconcomp.2006.11.004>

- Frangopol, D. M., & Liu, M. (2007). Maintenance and management of civil infrastructure based on condition, safety, optimization, and life-cycle cost. *Structure and Infrastructure Engineering*, 3(1), 29–41. <https://doi.org/10.1080/15732470500253164>
- Gallardo, A., & Román, J. S. (1993). Synthesis and characterization of a new poly(methacrylamide) bearing side groups of biomedical interest. *Polymer*, 34(2), 394–400. [https://doi.org/10.1016/0032-3861\(93\)90095-R](https://doi.org/10.1016/0032-3861(93)90095-R)
- Geib, D., & Singh, M. P. (2003). *Multiplexing of Extrinsic Fabry-Perot Optical Fiber Sensors for Strain Measurements*.
- Gong, H., Kizil, M. S., Chen, Z., Amanzadeh, M., Yang, B., & Aminossadati, S. M. (2019). Advances in fibre optic based geotechnical monitoring systems for underground excavations. *International Journal of Mining Science and Technology*, 29(2), 229–238. <https://doi.org/10.1016/j.ijmst.2018.06.007>
- Guo, H., Xiao, G., Mrad, N., & Yao, J. (2011, April). Fiber optic sensors for structural health monitoring of air platforms. *Sensors*, Vol. 11, pp. 3687–3705. <https://doi.org/10.3390/s110403687>
- Gyeongcheol Choe, Yasuji Shinohara, Gyuyong Kim, Sangkyu Lee, Euibae Lee, Jeongsoo Nam (2020). Concrete Corrosion Cracking and Transverse Bar Strain Behavior in a Reinforced Concrete Column under Simulated Marine Conditions. *Applied Sciences*. Vol. 10. pp. 1794-1807. <https://doi.org/10.3390/app10051794>.
- Handawi, K. Al, Vahdati, N., Shiryayev, O., & Lawand, L. (2017). Analytical modeling tool for design of hydrocarbon sensitive optical fibers. *Sensors (Switzerland)*, 17(10). <https://doi.org/10.3390/s17102227>
- Hansson, C. M. (2016). An introduction to corrosion of engineering materials. In *Corrosion of Steel in Concrete Structures* (pp. 3–18). <https://doi.org/10.1016/B978-1-78242-381-2.00001-8>
- Hao, H. (2016). Mechanics of Structures and Materials XXIV. In *Mechanics of Structures and Materials XXIV*. <https://doi.org/10.1201/9781315226460>
- Himour, A., Abderrahmane, S., Beliardouh, N. E., Zahzouh, M., & Ghers, M. (2005). Optical-fiber corrosion sensor based on deposit of Au/Ni-P. *Japanese Journal of Applied Physics, Part 1: Regular Papers and Short Notes and Review Papers*, 44(9 A), 6709–6713. <https://doi.org/10.1143/JJAP.44.6709>
- Huang, Z., Wu, C., Wang, Z., Wang, J., & Liu, L. (2018). Distributed measurement of axes misaligned splicing and multi-stress in polarization-maintaining fiber based on polarization-OTDR. *Optics Communications*, 423, 96–99. <https://doi.org/10.1016/j.optcom.2018.04.027>
- Hui, S. (Rob), Charlebois, L., & Sun, C. (2018). Real-time monitoring for structural health, public safety, and risk management of mine tailings dams. *Canadian Journal of Earth Sciences*, 55(3), 221–229. <https://doi.org/10.1139/cjes-2017-0186>

- John X.J.Zhang & KazunoriHoshino (2019). Chapter 5 - Optical transducers: Optical molecular sensing and spectroscopy. *Molecular Sensors and Nanodevices (Second Edition)*. pp. 231-309. <https://doi.org/10.1016/B978-0-12-814862-4.00005-3>.
- J.S. Carlton FR Eng (2019). Full-Scale Trials and Measurement Techniques. *Marine Propellers and Propulsion (Fourth Edition)*. 409-423. <https://doi.org/10.1016/B978-0-08-100366-4.00017-1>
- Kersey, A. D., Davis, M. A., Patrick, H. J., LeBlanc, M., Koo, K. P., Askins, C. G., ... Friebale, E. J. (1997). Fiber grating sensors. *Journal of Lightwave Technology*, 15(8), 1442–1463. <https://doi.org/10.1109/50.618377>
- Khechai, A., Tati, A., Guerira, B., Guettala, A., & Mohite, P. M. (2018). Strength degradation and stress analysis of composite plates with circular, square and rectangular notches using digital image correlation. *Composite Structures*, 185, 699–715. <https://doi.org/10.1016/j.compstruct.2017.11.060>
- Kim, B., & Peppas, N. A. (2002). Complexation phenomena in pH-responsive copolymer networks with pendent saccharides. *Macromolecules*, 35(25), 9545–9550. <https://doi.org/10.1021/ma0212011>
- Koleva, D. A., Wit, J. H. W. De, Breugel, K. Van, & Lodhi, Z. F. (2007). Investigation of Corrosion and Cathodic Protection in Reinforced Concrete I . Application of Electrochemical Techniques. *Journal of The Electrochemical Society*, 52–61. <https://doi.org/10.1149/1.2436609>
- Landolfo, R., Cascini, L., & Portioli, F. (2010). Modeling of metal structure corrosion damage: A state of the art report. *Sustainability*, 2(7), 2163–2175. <https://doi.org/10.3390/su2072163>
- Leng, J., & Asundi, A. (2003). Structural health monitoring of smart composite materials by using EFPI and FBG sensors. *Sensors and Actuators, A: Physical*, 103(3), 330–340. [https://doi.org/10.1016/S0924-4247\(02\)00429-6](https://doi.org/10.1016/S0924-4247(02)00429-6)
- Lin, X., Peng, M., Lei, F., Tan, J., & Shi, H. (2017). Analytical model of cracking due to rebar corrosion expansion in concrete considering the structure internal force. *AIP Advances*, 7(12). <https://doi.org/10.1063/1.5016454>
- Liu, X., Zhang, X., Cong, J., Xu, J., & Chen, K. (2003). Demonstration of etched cladding fiber Bragg grating-based sensors with hydrogel coating. *Sensors and Actuators, B: Chemical*, 96(1–2), 468–472. [https://doi.org/10.1016/S0925-4005\(03\)00605-1](https://doi.org/10.1016/S0925-4005(03)00605-1)
- López-Higuera, J. M., Cobo, L. R., Incera, A. Q., & Cobo, A. (2011). Fiber optic sensors in structural health monitoring. *Journal of Lightwave Technology*, 29(4), 587–608. <https://doi.org/10.1109/JLT.2011.2106479>
- Luciano, B., Ariel, G. F., Cardona, A., Kohan, P. H., Quinteros, R. D., & Storti, M. A. (2012). *Mecánica Computacional Vol XXXI*. Retrieved from <http://www.bioingenieria.edu.ar>

- Lyons, E. R., & Lee, H. P. (1999). Demonstration of an etched cladding fiber Bragg grating filter with reduced tuning force requirement. *IEEE Photonics Technology Letters*, 11(12), 1626–1628. <https://doi.org/10.1109/68.806868>
- L. Dorogin & B.N.J. Persson (2018). Contact mechanics for Polydimethylsiloxane: from liquid to solid. *Soft Matter* 14(4). <https://doi.org/10.1039/C7SM02216F>.
- Mahdavinia, G. R., Pourjavadi, A., Hosseinzadeh, H., & Zohuriaan, M. J. (2004). Modified chitosan 4. Superabsorbent hydrogels from poly(acrylic acid-co-acrylamide) grafted chitosan with salt- and pH-responsiveness properties. *European Polymer Journal*, 40(7), 1399–1407. <https://doi.org/10.1016/j.eurpolymj.2004.01.039>
- Majumder, M., Gangopadhyay, T. K., Chakraborty, A. K., Dasgupta, K., & Bhattacharya, D. K. (2008, September 15). Fibre Bragg gratings in structural health monitoring-Present status and applications. *Sensors and Actuators, A: Physical*, Vol. 147, pp. 150–164. <https://doi.org/10.1016/j.sna.2008.04.008>
- Maria Cristina Tanzi, Silvia Fare & Gabriele Candiani (2019). Chapter 5 - Sterilization and Degradation. *Foundations of Biomaterials Engineering*, pp. 289-328. <https://doi.org/10.1016/B978-0-08-101034-1.00005-0>.
- Mamoona Zaheer & Muhammad Shahid (2019). In-Situ Corrosion Monitoring Under Flowing Conditions; A Review. *Sci. Int*, 31(2), pp. 325-330.
- Measures, R. M. (2001). *Structural monitoring with fiber optic technology*. Academic.
- Méndez, A., & Csipkes, A. (2012). Overview of fiber optic sensors for NDT applications. *RILEM Bookseries*, 6, 179–184. https://doi.org/10.1007/978-94-007-0723-8_26
- Mishra, V., Lohar, M., & Amphawan, A. (2016). Improvement in temperature sensitivity of FBG by coating of different materials. *Optik*, 127(2), 825–828. <https://doi.org/10.1016/j.ijleo.2015.10.014>
- Muhammad Younus, Pankaj Chakrabarty & Mosharrafa Ahmad (2015). Optical Sensor based Efficient Internal Body Organ Monitoring. *International Journal of Computer Applications*. <https://doi.org/10.5120/21743-4966>
- Nishimura, R., & Maeda, Y. (2004). Stress corrosion cracking of type 304 austenitic stainless steel in sulphuric acid solution including sodium chloride and chromate. *Corrosion Science*, 46(2), 343–360. [https://doi.org/10.1016/S0010-938X\(03\)00154-9](https://doi.org/10.1016/S0010-938X(03)00154-9)
- Osada, Y., & Ross-Murphy, S. B. (1993). Intelligent Gels. *Scientific American*, 268(5), 82–87. <https://doi.org/10.1038/scientificamerican0593-82>
- Overload Failures. (2018). In *Failure Analysis and Prevention* (pp. 671–699). <https://doi.org/10.31399/asm.hb.v11.a0003543>

- Parhi, R. (2017). Cross-linked hydrogel for pharmaceutical applications: A review. *Advanced Pharmaceutical Bulletin*, Vol. 7, pp. 515–530. <https://doi.org/10.15171/apb.2017.064>
- Paulo Roriz, Susana Silva, Orlando Frazao & Susana Novais (2020). Optical Fiber Temperature Sensors and Their Biomedical Applications. *Sensors*. 20(7), 2113. <https://doi.org/10.3390/s20072113>
- Pereira, G. F. (2016). Fibre bragg grating as a multi-stage structure health monitoring sensor. In *MARE-WINT: New Materials and Reliability in Offshore Wind Turbine Technology* (pp. 53–66). https://doi.org/10.1007/978-3-319-39095-6_4
- Popoola, L. T., Grema, A. S., Latinwo, G. K., Gutti, B., & Balogun, A. S. (2013, December 1). Corrosion problems during oil and gas production and its mitigation. *International Journal of Industrial Chemistry*, Vol. 4. <https://doi.org/10.1186/2228-5547-4-35>
- Rahim, N. A. A., McDaniel, W., Bardon, K., Srinivasan, S., Vickerman, V., So, P. T. C., & Moon, J. H. (2009). Conjugated polymer nanoparticles for two-photon imaging of endothelial cells in a tissue model. *Advanced Materials*, 21(34), 3492–3496. <https://doi.org/10.1002/adma.200900416>
- Raul Davalos-Monteiro (2019). Observations of Corrosion Product Formation and Stress Corrosion Cracking on Brass Samples Exposed to Ammonia Environments. *Material Research*. <http://orcid.org/0000-0003-3058-5145>.
- Rhodes, P. R. (2001). Stress Corrosion Cracking of Austenitic Stainless Steels in. *Corrosion*, 5(11), 70654. <https://doi.org/10.5006/0010-9312-25.11.462>
- Rios, R., Magnin, T., Noel, D., & de Bouvier, O. (1995). Critical analysis of alloy 600 stress corrosion cracking mechanisms in primary water. *Metallurgical and Materials Transactions A*, 26(4), 925–939. <https://doi.org/10.1007/BF02649089>
- Sadrayi, A., Saffarzadeh, M., & Boroujerdian, A. M. (2019). RETRACTED ARTICLE: Assessment of Pedestrian Refuge Islands on Vehicle Speed Changes and Pedestrian Safety: Case Study in Tehran. *International Journal of Civil Engineering*, 17(5), 657–657. <https://doi.org/10.1007/s40999-017-0244-1>
- Sawpan, M. A., Pickering, K. L., & Fernyhough, A. (2011). Effect of fibre treatments on interfacial shear strength of hemp fibre reinforced polylactide and unsaturated polyester composites. *Composites Part A: Applied Science and Manufacturing*, 42(9), 1189–1196. <https://doi.org/10.1016/j.compositesa.2011.05.003>
- Schenato, L. (2017, September 1). A review of distributed fibre optic sensors for geo-hydrological applications. *Applied Sciences (Switzerland)*, Vol. 7. <https://doi.org/10.3390/app7090896>
- Serpe, M. J., Jones, C. D., & Lyon, L. A. (2003). Layer-by-Layer Deposition of Thermoresponsive Microgel Thin Films. *Langmuir*, 19(21), 8759–8764. <https://doi.org/10.1021/la034391h>

- Shoji, T., Lu, Z., & Peng, Q. (2011). Factors affecting stress corrosion cracking (SCC) and fundamental mechanistic understanding of stainless steels. *In Stress corrosion cracking: Theory and practice* (pp. 245–272). <https://doi.org/10.1533/9780857093769.3.245>
- Shuhui Liu, Shaoqing Cao, Zhe Zhang, Ying Wang, Changrui Liao & Yiping Wang. Temperature Sensor Based on Side-Polished Fiber SPR Device Coated with Polymer. *Sensors* 19(19),4063. <https://doi.org/10.3390/s19194063>.
- Strain Measurement with Fiber Bragg Grating Sensors | HBM. (n.d.). Retrieved September 3, 2019, from <https://www.hbm.com/en/3189/strain-measurement-with-fiber-bragg-grating-sensors/>
- Surre, F., Sun, T., & Grattan, K. T. (2013). Fiber optic strain monitoring for long-term evaluation of a concrete footbridge under extended test conditions. *IEEE Sensors Journal*, 13(3), 1036–1043. <https://doi.org/10.1109/JSEN.2012.2234736>
- Tan, Cai Hui, Mahamd Adikan, F. R., Shee, Y. G., & Yap, B. K. (2017). Non-destructive fiber Bragg grating based sensing system: Early corrosion detection for structural health monitoring. *Sensors and Actuators, A: Physical*, 268, 61–67. <https://doi.org/10.1016/j.sna.2017.10.048>
- Vaclav Prajzler, Woohyun Jung, Kyunghwan Oh, Jakub Cajzl & Pavla Nekvindova. Optical properties of deoxyribonucleic acid thin layers deposited on an elastomer substrate. *Optical Materials Express*, 1(2). <https://doi.org/10.1364/OME.10.000421>.
- Wang, Z. (2011). Polydimethylsiloxane Mechanical Properties Measured by Macroscopic Compression and Nanoindentation Techniques. *Graduate Theses and Dissertations*. Retrieved from <https://scholarcommons.usf.edu/etd/3402>
- Wu, H., Chiu, D. T., Anderson, J. R., Duffy, D. C., Whitesides, G. M., McDonald, J. C., & Schueller, O. J. (2000). Fabrication of microfluidic systems in poly(dimethylsiloxane). *Electrophoresis*, Vol. 21, pp. 27–40. [https://doi.org/10.1002/\(SICI\)1522-2683\(20000101\)21:1<27::AID-ELPS27>3.0.CO;2-C](https://doi.org/10.1002/(SICI)1522-2683(20000101)21:1<27::AID-ELPS27>3.0.CO;2-C) [pii] 10.1002/(SICI)1522-2683(20000101)21:1<27::AID-ELPS27>3.0.CO;2-C
- Yan, B., Li, J., Zhang, M., Zhang, J., Qiao, L., & Wang, T. (2019). Raman Distributed Temperature Sensor with Optical Dynamic Difference Compensation and Visual Localization Technology for Tunnel Fire Detection. *Sensors (Basel, Switzerland)*, 19(10). <https://doi.org/10.3390/s19102320>
- Ye, X. W., Su, Y. H., & Han, J. P. (2014). Structural health monitoring of civil infrastructure using optical fiber sensing technology: A comprehensive review. *Scientific World Journal*, Vol. 2014. <https://doi.org/10.1155/2014/652329>
- Ye, Z., Wang, J., Wang, C., & Jia, B. (2016). A positioning algorithm realized multilateration for distributed fiber-optic sensor. *Microwave and Optical Technology Letters*, 58(12), 2913–2917. <https://doi.org/10.1002/mop.30186>

- Yeo, T. L., Sun, T., Grattan, K. T. V., Parry, D., Lade, R., & Powell, B. D. (2005). Characterisation of a polymer-coated fibre Bragg grating sensor for relative humidity sensing. *Sensors and Actuators, B: Chemical*, 110(1), 148–156. <https://doi.org/10.1016/j.snb.2005.01.033>
- Yoon, H. J., Song, K. Y., Kim, J. S., & Kim, D. S. (2011). Longitudinal strain monitoring of rail using a distributed fiber sensor based on Brillouin optical correlation domain analysis. *NDT and E International*, 44(7), 637–644. <https://doi.org/10.1016/j.ndteint.2011.07.004>
- Yun, B., Chen, N., & Cui, Y. (2007). Highly sensitive liquid-level sensor based on etched fiber bragg grating. *IEEE Photonics Technology Letters*, 19(21), 1747–1749. <https://doi.org/10.1109/LPT.2007.905093>
- Zaghloul, M. A. S., Yan, A., Chen, R., Li, M. J., Flammang, R., Heibel, M., & Chen, K. P. (2017). High Spatial Resolution Radiation Detection Using Distributed Fiber Sensing Technique. *IEEE Transactions on Nuclear Science*, 64(9), 2569–2577. <https://doi.org/10.1109/TNS.2017.2735546>
- Zeng, L., Liu, Y., Zhang, G., Tang, L., Jiang, Z., & Liu, Z. (2017). Analysis of structural responses of bridges based on long-term structural health monitoring. *Mechanics of Advanced Materials and Structures*, 25(1), 1–8. <https://doi.org/10.1080/15376494.2016.1243283>
- Zhang, B. (2013). Development of sandglass shape FBG sensor to reduce cross sensitivity effect. *International Journal of Optics*, 2013. <https://doi.org/10.1155/2013/636987>
- Zhongde Dai, Luca Ansaloni & Liyuan Deng (2016). Recent advances in multi-layer composite polymeric membranes for CO₂ separation: A review. *Journal of Green Energy & Environment*, 2016. <https://doi.org/10.1016/j.gee.2016.08.001>

LIST OF PUBLICATIONS AND PAPERS PRESENTED

Journal Publications:

- (i) **Cai Hui Tan**, Faisal Rafiq Mahamad Adikan, Yu Gang Shee and Boon Kar Yap. Non-Destructive Fiber Bragg Grating based Sensing System: Early Corrosion Detection for Structural Health Monitoring. Science Direct: Sensors and Actuators A: Physical vol. 268 (2017), pg.61-67.
- (ii) **C.H. Tan**, Y.G. Shee, B.K Yap and F.R. Mahamd Adikan. Fiber Bragg Grating Based Sensing System: Early Corrosion Detection for Structural Health Monitoring. Science Direct: Sensors and Actuators A: Physical vol. 246 (2016), pg.123-128.
- (iii) **C.H Tan**, B. K Yap and F. R. Mahamd Adikan. HF Etched Fiber Bragg Grating To Detect Ethanol Concentrations. Journal of Engineering and Applied Sciences, 11 (2016), pg 1377-1378.

Conference attended

- (i) International Conference on Engineering & Technology, Computer, Basic & Applied Sciences (ECBA) 2015, Singapore.
- (ii) 2nd International Conference on Science and Engineering of Materials (ICoSEM) 2015, Kuala Lumpur.